

LIBRARY
ROYAL AIRCRAFT ESTABLISHMENT
BEDFORD.

R. & M. No. 3224



MINISTRY OF AVIATION

AERONAUTICAL RESEARCH COUNCIL
REPORTS AND MEMORANDA

The Effect of a Central Jet on the Base Pressure of a Cylindrical After-body in a Supersonic Stream

By J. REID and R. C. HASTINGS

LONDON: HER MAJESTY'S STATIONERY OFFICE

1961

PRICE: 17s. 6d. NET

R. & M. No. 3224

The Effect of a Central Jet on the Base Pressure of a Cylindrical After-body in a Supersonic Stream

By J. REID and R. C. HASTINGS

COMMUNICATED BY THE DEPUTY CONTROLLER AIRCRAFT (RESEARCH AND DEVELOPMENT),
MINISTRY OF AVIATION

*Reports and Memoranda No. 3224**

December, 1959

Summary. This Report describes an experimental investigation of the factors affecting the base flow and jet structure behind a cylindrical after-body with a central nozzle. Seven interchangeable nozzles were tested. Six of these were convergent-divergent, with a design Mach number of 2.0, jet/base diameter ratios ranging from 0.2 to 0.8 and nozzle divergence angles ranging from 0 deg to 10 deg. The seventh nozzle was convergent with a jet/base diameter ratio of 0.6.

In the main experimental programme the free-stream Mach number was 2.0 and the boundary layer was turbulent both on the after-body and in the nozzle. Measurements were made of the base pressure, the surface pressure distribution inside the nozzle, the overall thrust and the nozzle mass flow, over a range of jet pressures. This programme was supplemented by comparative tests with the jet exhausting into still air (static tests). Readings were taken of the internal nozzle pressures and the jet thrust at different jet pressures. Schlieren photography was used extensively throughout.

The results of the tests with external flow are presented in the form of curves showing the separate effects of jet pressure ratio, jet/base diameter ratio, nozzle design Mach number and nozzle divergence angle on the base pressure and overall thrust. The special case of base bleed is discussed separately. Similar curves are included for the static tests. These show the effect of jet pressure ratio and nozzle geometry on the jet thrust.

A general method of correlating data on annular base pressures is proposed and discussed. Essentially, this method compares the pressure on an annular base with the calculated pressure on the corresponding two-dimensional base. It correlates the present results reasonably well, but is less successful when applied to more extensive data.

1. *Introduction.* The experimental work described in this Report is mainly concerned with the factors affecting the pressure on an annular base separating two supersonic streams. This is a problem which arises naturally when considering the integrated design of an engine nacelle and, for this reason, it has received considerable attention in recent years. What is most needed from the design aspect is a fairly rapid and reasonably accurate method of predicting the base pressure on a given configuration under given operating conditions. If this were available the selection, on a thrust-minus-drag basis, of the optimum design for a given cruising speed, and the estimation of its performance at off-design conditions, would be a relatively simple matter. The solution of this problem has, however, proved elusive.

The most promising theoretical approach is best considered with reference to the schematic flow diagram shown in Fig. 1. The outer and inner streams leave the surface at A and B respectively and

* Previously issued as R.A.E. Report No. Aero. 2621—A.R.C. 21,796.

transfer momentum to the fluid behind the base by turbulent mixing. (We need consider only the practical case in which both boundary layers are turbulent.) To preserve continuity, the flow dividing lines AC and BC which, respectively, separate the outer and inner flows from the trapped flow, must meet at a point C, which will be a stagnation point. The trapped air must therefore circulate, probably as a pair of eddies, and the pressure rise required to preserve this circulatory flow is provided by the trailing shocks at C.

Now in the analogous, but simpler case of a two-dimensional backward-facing step, Beastall and Eggink¹ showed experimentally that, provided the boundary layer is turbulent and thin compared with the step height, the pressure ratio across the trailing shock depends only on the Mach number just upstream of the shock. Moreover, this concept of a 'critical' pressure rise appears to be fundamental, and is applicable in a slightly extended form to the general two-dimensional problem in which a base separates two streams, inclined to one another, and of different Mach number and total pressure. In this case Cortright² assumes that the common pressure ratio across the trailing shocks is the same unique function of the *mean* of the Mach numbers of the two streams just ahead of the shocks, and hence calculates the base pressure. Fair agreement with the experimental evidence is obtained over quite a wide range.

In principle this method is also applicable to the annular base shown in Fig. 1, but in this case the streamlines AC and BC (which, in two dimensions, are straight before re-compression) have to be determined by iterative methods using axi-symmetric characteristics. This process is too laborious for the method to be of practical value.

In view of the theoretical difficulties it is natural to resort to experiment, but here the obstacle is the number of independent variables. Using the notation of Fig. 2 and the 'List of Symbols' of this Report, and assuming that both boundary layers are turbulent and thin, we may write:

$$\frac{p_B}{p_1} = f\left(M_1, M_2, \beta_1, \beta_2, \frac{d_2}{d_1}, \frac{i p_2}{i p_1}\right). \quad (1)$$

There are thus six independent variables, and although systematic experimental data on the separate effects of these variables has been published³, it is, as a rule, too scanty to permit accurate interpolation, and is likely to remain so.

In these circumstances the present authors propose the concept of correlating the pressure on an annular base with the (calculated) pressure on the 'corresponding' two-dimensional base. By 'corresponding' we mean that the two profiles are congruent in section and that M_1 , M_2 and $i p_2 / i p_1$ are identical in the two cases.

If, for brevity, we define:

$$(p_B/p_1)_2^3 = (p_B/p_1)_3 / (p_B/p_1)_2$$

where $(p_B/p_1)_3$ refers to the annular base

and $(p_B/p_1)_2$ refers to the corresponding two-dimensional base.

Then,

$$(p_B/p_1)_2^3 = F\left(M_1, M_2, \beta_1, \beta_2, \frac{d_2}{d_1}, \frac{i p_2}{i p_1}\right). \quad (2)$$

Formally, Equation (2) is no simpler than Equation (1), but as $d_2/d_1 \rightarrow 1$, $(p_B/p_1)_3 \rightarrow (p_B/p_1)_2$ so that $(p_B/p_1)_2^3 \rightarrow 1$. Hence $(p_B/p_1)_2^3$ is independent of M_1 , M_2 , β_1 , β_2 and $i p_2 / i p_1$ when $d_2/d_1 = 1$ and we might reasonably expect it to be insensitive to these five variables provided that d_2/d_1 is not

too far removed from unity. Graphically this is equivalent to saying that when $(p_B/p_1)_2^3$ is plotted against d_2/d_1 all the points may be expected to lie on, or close to, a curve through the point (1, 1).

The present experiments were designed primarily to find out whether there exists, to a sufficient degree of approximation, a unique correlation curve of this type and, if so, to determine its shape. In the course of this work additional data were obtained on the overall thrust of the various configurations, the effect of base bleed on the base drag* and the influence of jet pressure ratio on the jet structure, both with and without external flow. Each of these matters is discussed in detail in the appropriate section of the Report.

2. *Description of Wind Tunnel and Models.* 2.1. *The Tunnel.* The experiments were made in a supersonic tunnel (No. 16) specifically designed for the purpose. This tunnel, which has been described in detail in a previous report⁴ and is illustrated in Fig. 3, is of the open-circuit, open-jet type.

The supersonic nozzle ($M = 2.0$) is axi-symmetric and the model under test is screwed to the end of a long, double-skinned, cylindrical tube (the centre-body) which is mounted co-axial with the nozzle and passes through the nozzle throat and settling chamber into a separate plenum chamber. The main air supply for the internal jet passes from this plenum chamber through a slotted drum and thence *via* the centre-body to the model. Pressure lines from the model pass between the two skins of the centre-body to a multi-point connector and thence through the wall of the nozzle settling chamber to a bank of mercury manometers. Interference caused either by model supports or pressure leads is thus eliminated.

The complete central assembly comprising the slotted drum, centre-body and model is supported by three sets of ball bearings and is free to slide axially between limit stops. A simple device consisting of a piston and cylinder in which the thrust is balanced automatically by hydraulic pressure serves to measure the axial force on the central assembly. To obtain the axial force on the model itself, corrections must be applied to the observed thrust in order to compensate for out of balance pressures in the different tunnel chambers, although the pressure balance pipe shown in Fig. 3 serves to reduce these to a minimum. No correction is required for inlet momentum as the air enters the slotted drum radially. The hydraulic balance was calibrated directly by weights at frequent intervals but no change in the calibration could be detected throughout the experiment.

Air for the main tunnel flow is taken from the atmosphere, dried chemically and heated electrically to about 20 deg C, and then delivered to the settling chamber at slightly less than atmospheric stagnation pressure. Normally the internal jet was fed, *via* the slotted drum, with undried atmospheric air compressed to 2 Atm abs. and then cooled to about 20 deg C, the supply pressure being controlled by a valve and bleed. With this supply system the total and static pressures were measured in the centre-body just upstream of the model, but no direct measurement was made of the mass flow. An alternative method of supply was, however, adopted for the experiments on base bleed, in which the accurate measurement and control of small mass flows was essential. In these tests the centre-body and model were isolated from the main supply by a blank (*see* Fig. 3) and undried atmospheric air was supplied directly to the internal nozzle through a small auxiliary pipe. A sharp-edged metering orifice served to measure the mass flow. By this means errors in mass flow measurement due to unavoidable leakage through the glands in the

* In the experiments on base bleed the central nozzle was used as the bleed duct. No attempt was made to bleed air separately into the base annulus with the central jet in operation.

plenum chamber were avoided. Other possible sources of leakage were carefully sealed with rubber cement or shellac, and the entire auxiliary supply system was tested by evacuation before each experiment. These precautions were essential because the base pressure is very sensitive to bleed mass flow.

As the air fed to the internal nozzle was not dried, the exit Mach number varied slightly with atmospheric humidity. The variation (about ± 1 per cent of the mean) had no significant effect on the base pressure.

A conventional two-mirror schlieren system with a continuous light source provided visualisation of the flow. Extensive records of the various types of flow pattern were taken using a magazine film camera with an exposure of 0.01 sec.

The test conditions and the leading tunnel dimensions are listed below:

Tunnel dimensions

Exit diameter of supersonic nozzle = .11 in.

Diameter of centre-body = 3.9 in.

Test conditions

(a) *External stream*

Stagnation pressure = 0.84 Atm abs. (25 in. Hg abs.)

Stagnation temperature = 20 deg C

Mach number = 2.02

Reynolds number = 2.7×10^5 per inch

State of boundary layer on centre-body. Turbulent.

(b) *Internal stream*

Maximum stagnation pressure = 2.0 Atm abs. (60 in. Hg abs.)

Stagnation temperature = 20 deg C

State of boundary layer. Turbulent.

All tests with the internal nozzle exhausting into still air were made at an ambient static pressure of 0.1 Atm abs. (3 in. Hg abs.).

2.2. *The Models.* A cylindrical after-body ($\beta_1 = 0$ deg) with seven interchangeable nozzles was selected for investigation. Fig. 4 (a to g) shows the leading dimensions of the models and the range of variables covered is summarised in the following table.

TABLE 1

Code No.	M_2^*	β_2 (deg)	d_2/d_1
2-5-20	2.0	5	0.2
2-5-40	2.0	5	0.4
2-5-60	2.0	5	0.6
2-5-80	2.0	5	0.8
2-10-60	2.0	10	0.6
1-0-60	1.0	0	0.6
2-0-60	2.0	0	0.6

(Each model is identified by a code number. The key to the code will be evident from the table.)

The models form the following three groups, in each of which one only of the three parameters is systematically varied.

Group 1 Models 2-5-20 (40) (60) (80)
Group 2 Models 1 (2) -0-60
Group 3 2-0 (5) (10) -60

These three groups served to investigate the respective effects of d_2/d_1 , M_2^* and β_2 on the base pressure.

The five nozzles which have a finite divergence angle ($\beta_2 = 5$ deg or 10 deg) were designed with M_2^* equal to 2.0. In meridian section each nozzle profile was formed by two straight lines joined tangentially by a circular arc of radius equal to the throat diameter. With under-expanded flow the surface pressure distribution inside these nozzles corresponded closely with that predicted by one-dimensional isentropic theory and there was no indication of internal disturbances on the schlieren photographs. (See Fig. 10.)

The supersonic nozzle with zero divergence angle (2-0-60) was designed to give uniform parallel flow at Mach number 2.0 in the exit plane. The co-ordinates were obtained by interpolation from tabulated data. When under-expanded, the flow produced by this nozzle appeared to be shock free (see Figs. 6 and 19), and the internal surface pressure distribution agreed well with that calculated from the characteristics net. (See Figs. 8 and 18.)

The sonic nozzle (1-0-60) was formed by a straight approach section joined to a short straight throat section by a circular arc of large radius. Schlieren photographs of the flow are shown in Figs. 12 and 20.

All the models were turned from solid mild steel bar. The internal contours were bored in a profiling lathe to a hand-made template, and both dimensional accuracy and quality of surface finish were uniformly high.

Each of the models was provided with static pressure points on the external and internal surfaces and on the base, as shown in Fig. 4 (a to g). In addition, the stagnation and static pressures of the internal flow just upstream of the throat were measured by a pitot tube (on the axis of symmetry) and static tube (half-way across a radius).

3. Details of the Experiment. 3.1. Preliminary Tests.

3.1.1. *The elimination of external interference.* Before starting the main experiments it was necessary to choose a position for the model in the working section such that the expansion fan from the lip of the tunnel nozzle did not affect the base pressure. Previous work⁴ had shown that, in the case of a sealed axi-symmetric base, a disturbance-free wake some five base radii in length is required to eliminate interference completely. When, however, air is bled into the base region, the base pressure increases (see Fig. 5) and the trailing shock moves downstream, so that at the peak base pressure the criterion for interference-free flow is likely to be more stringent.

To guard against possible errors from this cause preliminary tests were made with the model 2-10-60 situated at two different axial positions in the test section, designated $l = 13.6$ in. and $l = 18.9$ in. (see List of Symbols). In each position the effect of bleed flow on base pressure was measured over a range which included the peak base pressure. As the two curves agreed closely, it was concluded that the effect of external interference was insignificant in either position, and all subsequent pressure and thrust measurements were made with $l = 18.9$ in. The schlieren photographs which, of necessity, were taken with $l = 24.8$ in. are affected slightly by interference in the region of the base pressure peak.

3.1.2. *The state of the boundary layers.* In a previous set of experiments⁴ the velocity profile of the boundary layer on the external surface of the centre-body was measured at a number of axial stations. These data show that, with the model in the standard position for the present tests ($l = 18.9$ in.), the external boundary layer is turbulent, with the displacement thickness $\delta^* = 0.0490$ in., the momentum thickness $\theta = 0.0165$ in. and $\delta^*/\theta = 2.97$ in the base plane.

To determine the characteristics of the internal boundary layer the velocity profile was measured 0.15 in. upstream of the exit plane on model 2-5-60 using a flattened pitot tube 0.006 in. thick. For this test the jet was run at a stagnation pressure of 1.8 Atm abs., exhausting into still air at a static pressure of 0.1 Atm abs. The measured velocity profile was typical of a turbulent boundary layer and was, in fact, practically identical (when plotted in non-dimensional form) with that previously obtained on the external surface of the centre-body. Numerical integration of the profile gave $\delta^* = 0.0103$ in., $\theta = 0.0037$ in. and $\delta^*/\theta = 2.78$.

It will be noted that these data were obtained with a relatively large nozzle ($d_2/d_1 = 0.6$) operating at a high stagnation pressure. It is possible that with a smaller nozzle or a lower stagnation pressure the internal boundary layer might be laminar, although this is considered to be unlikely.

3.2. *Tests with External Flow ($M_1 = 2.0$).* With each model measurements were made of the base pressure (p_B), the static reference pressure on the after-body (p_1), and the surface pressure distribution inside the central nozzle at a number of closely spaced values of jet stagnation pressure ($i p_2$) ranging from that corresponding to zero mass flow to 2 Atm abs., the tunnel stagnation pressure ($i p_1$) being maintained constant at 0.84 Atm abs. throughout. The points were normally taken in order of increasing jet pressure.

Over the lower part of the range in $i p_2$ the inner jet was fed through the auxiliary supply pipe mentioned in Section 2.1, and the mass flow measured by a sharp-edged metering orifice. The isolating blank (Fig. 3) was then removed, the auxiliary pipe sealed, and the main air supply to the inner jet brought into operation. Measurements of the net thrust were commenced at about $i p_2/i p_1 = 0.3$ and continued up to the maximum jet pressure.

After completion of these readings each model (except 2-10-60) was moved downstream to bring the base into the field of the schlieren system and a complete set of photographs taken covering the entire range of jet pressure. Normally the schlieren knife edge was set horizontal.

3.3. *Tests without External Flow ($M_1 = 0$).* The experiments described in the preceding section were supplemented by further tests with the central jet exhausting into still air at a static pressure (p_1) of 0.1 Atm abs. With each model (except 2-10-60) the thrust and the surface pressure distribution inside the nozzle were measured for values of $i p_2/p_1$ ranging from 1 to 20. A complete set of schlieren photographs was also taken to record the effect of jet pressure on the jet structure.

4. Discussion of Results. Tests with External Flow ($M_1 = 2.0$).

4.1. The Data on Base Pressure.

4.1.1. *The effect of jet pressure ratio ($i p_2/i p_1$) on base pressure.* The physical nature of the flow behind an annular base is brought out most clearly by considering in detail the effect of jet pressure ratio on the base pressure for a typical configuration (Model No. 2-0-60). The graph of p_B/p_1 against $i p_2/i p_1$ is shown in Fig. 5 and the corresponding set of schlieren photographs in Fig. 6. Schematic diagrams of the base flow are shown in Fig. 7 (a to f), and Fig. 8 illustrates the surface pressure distribution inside the nozzle. The following discussion is based partly on these four figures and partly on the results presented in Ref. 5.

Turning first to Fig. 5, the point (1) corresponds to the case of a sealed base. Under these conditions all the air entrained by the external stream is returned to the base region by the pressure rise across the trailing shock, and a closed circulating flow results as shown in Fig. 7a. Now when p_2 is increased, part of the entrained air is supplied by the internal jet so that the mass and momentum of the trapped circulating air decrease. Consequently the pressure rise necessary to return this trapped air to the base region decreases also and the base pressure rises. This trend continues until, at point (3), all the air entrained by the external flow is supplied by the internal jet so that the original eddy and trailing shock disappear. It is clear, however, that as the velocity of the internal jet increases a small pair of eddies will be created in the region bounded by the external and internal streams and the base. The flow pattern at point (3) will therefore be as shown in Fig. 7b. The corresponding curve ($p_2/p_1 = 0.104$) in Fig. 8 shows that the flow is still subsonic throughout the nozzle.

As p_2 is further increased the flow reaches sonic velocity in the nozzle throat ($M_0 = 1$ in Fig. 5) and thereafter a forked shock system causing separation from the nozzle wall forms downstream of the throat. The relevant flow pattern is shown in Fig. 7c. This shock system moves downstream with increasing jet pressure, as is shown by Fig. 8, in which separation corresponds to the point where the experimental curves branch off from the common curve. Finally, at point (6), the initial shock reaches the nozzle exit plane (see Fig. 7d). At this point $M_2 = 2.0$ but p_2 is less than p_B . (In Fig. 8 the theoretical pressure discontinuity across the shock is 'smoothed-out' by the boundary layer as is shown by the curve for $p_2/p_1 = 0.296$.) Thereafter the nozzle runs full, so that M_2 and p_2/p_2 are constant. Consequently, as p_2 is increased, p_2 increases also and the shock weakens until, at point (7), $p_2 = p_B$ and the internal flow is discharged parallel to the axis (Fig. 7e). Beyond this point p_2 rises above p_B and an expansion fan forms at the nozzle lip (Fig. 7f).

It is not profitable to attempt a detailed verbal analysis of the effect of these changes in flow pattern on the base pressure, except to point out the cause of the discontinuity in gradient of the base pressure curve (Fig. 5) at the point (10). The explanation lies in the shape of the shock formed downstream of the base in the internal flow. At high jet pressures this shock is forked and from the schlieren photographs in Fig. 6 it will be seen that, as p_2/p_1 decreases, the trailing branch of the fork moves closer to the leading branch. Referring then to Fig. 7f, let CD denote the region of compression due to the leading shock and EF denote the region of compression due to the trailing shock. When the jet pressure is large, E lies downstream of D and the trailing shock does not affect the base pressure. As, however, the jet pressure is decreased, the trailing shock moves upstream until a critical jet pressure is reached (corresponding to point (10) in Fig. 5) at which E coincides with D. When the jet pressure is less than this critical value, both the leading and trailing branches of the shock affect the base pressure and consequently there is a discontinuity in the gradient of the base pressure curve (Fig. 5) at the point (10). This phenomenon is analogous to the effect of an external shock on the base pressure of a sealed base as the disturbance is moved progressively upstream.

It is convenient for descriptive purposes to divide the base pressure curve shown in Fig. 5 into three parts; phase 1 (points (1) to (3)), phase 2 (points (3) to (10)) and phase 3 (points (10) to (18)). This method of division is suggested by the form of the curve but, as explained above, it also serves to emphasise fundamental differences in the physical nature of the flow*. Phase 1 is referred to as the 'base bleed' condition because the effluent is entrained rather than emitted as a jet.

* In a previous report on two-dimensional base flow⁵, no division was drawn between phases 2 and 3 because the physical difference between them was not, at that time, clearly appreciated.

4.1.2. *The effect of jet/base diameter ratio, d_2/d_1 on base pressure.* Fig. 9 shows p_B/p_1 plotted against $i p_2/i p_1$ treating d_2/d_1 as a parameter, for the four models 2-5-20 (40) (60) (80). It will be noted that each of these curves exhibits the three phases referred to in the preceding section.

Perhaps the most interesting feature of this family is the relative position of the four curves and, in particular, the behaviour of the maximum and minimum base pressures as d_2/d_1 tends to zero. The base pressure with no internal flow, which we will denote by $(p_B/p_1)_{Q=0}$ is, of course, independent of d_2/d_1 and physically we might expect that, as d_2/d_1 is decreased, the experimental curves would approach a horizontal straight line with the ordinate $(p_B/p_1)_{Q=0}$.

The maximum base pressure does, in fact, behave in this way. $(p_B/p_1)_{\max}$ varies almost linearly with d_2/d_1 and, as d_2/d_1 tends to zero, $(p_B/p_1)_{\max}$ tends to $(p_B/p_1)_{Q=0}$.

On the other hand, the minimum base pressure behaves quite differently. $(p_B/p_1)_{\min}$ appears to be practically independent of d_2/d_1 , although the value of $i p_2/i p_1$ corresponding to $(p_B/p_1)_{\min}$ increases progressively as d_2/d_1 decreases. It appears that however small the central jet may be, it can still exert a finite effect on the base pressure provided that the stagnation pressure is high enough.

Fig. 9 also illustrates a practical point. In current practice the convergent-divergent nozzle of a supersonic aircraft is often designed such that the jet exhausts at the free-stream static pressure, *i.e.*, such that $p_2 = p_1$. This criterion gives the maximum thrust at zero flight speed, when $p_B = p_1$. If, however, we consider an aircraft cruising at $M = 2.0$ and powered by a turbo-jet, we may take $i p_2/i p_1 = 1.3$ as a typical value. Under these conditions Fig. 9 shows, firstly, that a nozzle designed for $M_2 = 2.0$ would run under-expanded ($p_2 > p_B$) and, secondly, that the base pressure would be low. Both these factors detract from the overall thrust, and it is by no means certain that the $p_2 = p_1$ criterion corresponds to the optimum design with a finite base area in supersonic flight. Further reference to this point will be made in Section 4.2.

The irregularities in the curves for $d_2/d_1 = 0.4$ and 0.6 with over-expansion ($p_2 < p_B$) are probably due to the effect of slight irregularities in the nozzle profile on the position of the separation point inside the nozzle. They appear to have no fundamental significance.

Typical schlieren photographs showing the effect of d_2/d_1 on the base flow with $i p_2/i p_1 = 2.35$ are presented in Fig. 10.

4.1.3. *The effect of nozzle design Mach number (M_2^*) on base pressure.* Fig. 11, in which p_B/p_1 is plotted against $i p_2/i p_1$ for the two models 2-0-60 and 1-0-60, illustrates the effect of nozzle design Mach number on the base pressure. The corresponding schlieren photographs are shown in Figs. 6 and 12 respectively.

Comparing the two curves in Fig. 11 we note that, in phase 3, the base pressure with the sonic nozzle (1-0-60) is considerably greater than that obtained with the supersonic nozzle (2-0-60). This lower base drag with the sonic nozzle tends to compensate the loss in internal thrust caused by excessive under-expansion.

It will be seen also that with the sonic nozzle, in addition to the usual base pressure minimum separating phases 2 and 3 (which occurs at $i p_2/i p_1 = 0.29$) there exists also a secondary minimum at $i p_2/i p_1 = 0.19$. This secondary minimum differs from the irregularities observed with models 2-5-40 and 2-5-60 which were mentioned in Section 4.1.2 in that it occurs when the nozzle is under-expanded. An associated instability of the external shock system was noted on the schlieren but the cause and significance of this phenomenon are not clear.

4.1.4. *The effect of nozzle divergence angle (β_2) on base pressure.* Fig. 13 shows p_B/p_1 plotted against p_2/p_1 with β_2 as a parameter for the three models 2-0 (5) (10)-60. In so far as phase 3 is concerned it will be observed that p_B/p_1 tends to increase slightly with increase in β_2 . This trend is much more marked in the corresponding two-dimensional case in which the calculated value of p_B/p_1 increases rapidly and approximately linearly with β_2 .

Figs. 9, 11 and 13 provide the experimental basis for the method of correlation discussed in Section 6 and their significance will be analysed in more detail in that section.

4.2. *The Thrust and Drag Data.* We consider next the force measurements made with the seven models. In this connection, using the notation shown in Fig. 2 and noting that the after-body is cylindrical, we define the jet thrust coefficient $(C_T)_{\text{jet}}$ by the equation:

$$q_1 a_1 (C_T)_{\text{jet}} = Q u_2 + (p_2 - p_1) a_2 \quad (3)$$

and the base drag coefficient $(C_D)_{\text{base}}$ by the equation:

$$q_1 a_1 (C_D)_{\text{base}} = (p_1 - p_B) (a_1 - a_2) \quad (4)$$

where $q_1 = \frac{1}{2} \rho_1 u_1^2$.

The difference between these two coefficients, $[(C_T)_{\text{jet}} - (C_D)_{\text{base}}]$, which is of most direct interest from the practical viewpoint, was calculated from the balance readings, allowance being made for the effect of skin friction on the external surface of the cylinder and out-of-balance pressures in the difference tunnel chambers. (The constant skin-friction correction was obtained by measuring the drag and base pressure with no internal flow.) $(C_D)_{\text{base}}$ was obtained by averaging the measured distribution of pressure over the base area, and $(C_T)_{\text{jet}}$ then derived by addition.

For a nozzle of given geometry, running without internal separation, p_2 , u_2 and Q depend solely on p_2 so that, by definition, $(C_T)_{\text{jet}}$ at a given value of p_2/p_1 is the same either with or without external flow. This conclusion was confirmed by the experimental thrust measurements.

It follows that, with this restriction, the overall thrust coefficient in supersonic flight $[(C_T)_{\text{jet}} - (C_D)_{\text{base}}]$ may be calculated with sufficient accuracy from force measurements obtained without external flow (static tests) coupled with base pressure measurements made with external flow. This is an important practical point since the measurement of force with external flow requires specialised equipment and such data are consequently scarce.

In Fig. 14 $(C_T)_{\text{jet}}$, $(C_D)_{\text{base}}$ and $(C_T)_{\text{jet}} - (C_D)_{\text{base}}$ are plotted against p_2/p_1 treating d_2/d_1 as a parameter. These graphs are largely self-explanatory and call for no special comment.

In Fig. 15 a comparison is made of the jet thrust and base drag coefficients of a sonic nozzle and a supersonic nozzle ($M_2^* = 2.0$) with the same throat area ($d_0/d_1 = 0.6$), and hence equivalent mass flows. (The curves for the supersonic nozzle were obtained by interpolation from Fig. 14.) This comparison merits a brief discussion.

We note firstly, that at the higher pressure ratios the jet thrust coefficient $[(C_T)_{\text{jet}}]$ of the sonic nozzle is less than that of the supersonic nozzle. This is due simply to the fact that the sonic nozzle lacks a forward-facing surface for the pressure to act upon and is hence unable to convert a large proportion of the available pressure drop into thrust. On the other hand, $(C_D)_{\text{base}}$ is much the same for the two nozzles because, although the sonic nozzle has the higher base pressure (see Fig. 11), it has also the larger base area. Consequently, as shown in the bottom graph (Fig. 15), the overall thrust of the supersonic nozzle exceeds that of the sonic nozzle at all but the lowest values of jet pressure ratio.

These results are particularly interesting in that they throw some light on the important practical problem of thrust optimisation. To focus ideas we may restrict discussion to the case of a cylindrical after-body and state the problem in the following terms. Consider an aircraft which is to cruise at a prescribed speed, propelled by a nacelle-mounted turbo-jet engine of specified design. We may then take M_1 , d_1 , d_0 and p_2/p_1 (see Fig. 2) as known and we require to find d_2 and β_2 such that $(C_T)_{\text{jet}} - (C_D)_{\text{base}}$ is a maximum under cruising conditions. In current design practice the values of d_2 and β_2 chosen are those which make $(C_T)_{\text{jet}}$ a maximum under static conditions (*i.e.*, with no external flow). As explained in Section 4.1.2, this implies that the jet exhausts at the free stream static pressure ($p_2 = p_1$) and it is by no means certain that $(C_T)_{\text{jet}} - (C_D)_{\text{base}}$ is a maximum under these conditions in supersonic flight when the effect of the sub-ambient base pressure is taken into account. The present results are, of course, not sufficient to establish the required design criteria for optimum overall thrust in supersonic flight, but they do show that a convergent-divergent nozzle discharging at the free-stream static pressure gives more thrust than a plain convergent nozzle.

Fig. 16 shows the effect of jet pressure ratio on the jet thrust and base drag of three supersonic nozzles ($M_2^* = 2.0$) with nozzle divergence angles of 0 deg, 5 deg and 10 deg respectively. The comparison is made at a constant value of d_2/d_1 equal to 0.6.

Considering first the results for $(C_T)_{\text{jet}}$ shown in the top graph, we note that the curves for $\beta_2 = 0$ deg and 5 deg, which are practically identical, lie slightly above the curve for $\beta_2 = 10$ deg. This trend is presumably due to the increased radial momentum (and consequently decreased axial momentum) which accompanies an increase in the nozzle divergence angle. The middle graph shows, however, that when $\beta_2 = 10$ deg, $(C_D)_{\text{base}}$ also is slightly less than when $\beta_2 = 0$ deg or 5 deg (see Fig. 13). Consequently, as shown in the bottom graph (Fig. 16), the overall thrust coefficient $[(C_T)_{\text{jet}} - (C_D)_{\text{base}}]$ is independent of the nozzle divergence angle. This example illustrates in some measure the danger of neglecting the contribution of the base to the overall thrust since, on the basis of static tests (no external flow), the nozzle with $\beta_2 = 10$ deg would be judged slightly inferior to nozzles with $\beta_2 = 0$ deg or 5 deg.

4.3. *The Data on Base Bleed.* For some time it has been known⁵ that the introduction of a relatively small quantity of low-energy air into the 'dead' region behind a sealed base results in an increase in the base pressure. This procedure (base bleed) can, when properly controlled, lead to a substantial reduction in the base drag and, for this reason, is of considerable practical interest. The present tests, which were made on four models (2-5-20 (40) (60) (80)) using the central supersonic nozzle as the bleed duct, were designed to investigate the effect of the two primary design parameters, d_2/d_1 and the bleed mass flow (Q).

The results are shown in Fig. 17, in which p_B/p_1 is plotted, as is customary, against the non-dimensional 'bleed number' (H), which is proportional to Q . H was originally introduced by Korst⁶ for theoretical reasons. We note that when H is small p_B/p_1 increases linearly with H and is independent of d_2/d_1 . On the other hand, the peak base pressure $(p_B/p_1)_{\text{max}}$ decreases as d_2/d_1 decreases. Table 2 shows the effect of d_2/d_1 on the total drag coefficient $[(C_D)_{\text{base}} - (C_T)_{\text{jet}}]$. Bearing in mind that a correction is required for the intake drag of the bleed air, this coefficient is a measure of the combined drag of the base and bleed duct.

TABLE 2

d_2/d_1	0.2	0.4	0.6	0.8
$[(C_D)_{\text{base}} - (C_T)_{\text{jet}}]_{Q=0}$	0.151	0.151	0.151	0.151
$[(C_D)_{\text{base}} - (C_T)_{\text{jet}}]_{\text{min}}$	0.134	0.107	0.078	0.053
$\frac{[(C_D)_{\text{base}} - (C_T)_{\text{jet}}]_{\text{min}}}{[(C_D)_{\text{base}} - (C_T)_{\text{jet}}]_{Q=0}}$	0.887	0.709	0.517	0.351

Note

$[(C_D)_{\text{base}} - (C_T)_{\text{jet}}]_{Q=0}$ denotes the value of the total drag coefficient without base bleed.

$[(C_D)_{\text{base}} - (C_T)_{\text{jet}}]_{\text{min}}$ denotes the minimum value of the total drag coefficient with base bleed.

It is immediately apparent from this table (and Fig. 17) that base bleed is most effective when the area of the bleed duct is as large as possible. The reasons for this are apparent when we attempt to interpret Fig. 17 in physical terms.

As explained in Section 4.1.1, when the bleed flow is zero ($Q = 0$) the external flow transfers momentum to the air behind the base by a turbulent mixing process and hence accelerates it. To preserve continuity this entrained air is subsequently returned to the base region by a trailing shock, and a closed eddy flow results (see Fig. 7a). When bleed air is introduced with a very low axial velocity, part of the air entrained by the external stream is supplied by the bleed flow, so that less recompression is required to maintain the circulating flow, and the base pressure consequently rises. On this argument we would expect p_B/p_1 to depend only on H (or Q) provided that H is sufficiently small, and this conclusion is borne out by Fig. 17.

As H is increased, however, (d_2/d_1 being constant) the bleed velocity increases also and eventually a secondary pair of eddies is formed behind the base annulus. Further increase in H (and hence in bleed velocity) increases the momentum transferred by turbulent mixing to the secondary vortex pair. Consequently, the pressure rise through the associated shock increases also, and since the wake pressure behind this shock is sensibly constant, the base pressure drops. It is clear, therefore, that in order to obtain the most benefit from base bleed, the bleed air should be introduced with a sufficiently low axial velocity that a strong secondary pair of eddies is not formed behind the base annulus.

5. Discussion of Results. Tests without External Flow ($M_1 = 0$). 5.1. The Effect of Jet Pressure Ratio ($i p_2/p_1$) on the Jet Structure. It is of interest to examine, in some detail, the development of the flow pattern in a jet as the pressure ratio is gradually increased. Firstly we will consider the case of a supersonic jet using the results obtained with Model No. 2-0-60 as a typical example. Fig. 18 shows the change in surface pressure distribution inside the nozzle, and the schlieren photographs in Fig. 19 illustrate the development of the external jet structure.

It is clear that as $i p_2/p_1$ is increased the flow, which initially is subsonic throughout the nozzle, eventually reaches sonic velocity in the throat. This point is reached when $i p_2/p_1 = 1.4$ approximately (see Fig. 18). Thereafter, a shock causing separation from the nozzle wall forms downstream of the throat. This shock, by repeated reflection from the nozzle walls, gives rise to a forked system which is clearly visible in the schlieren photographs (Fig. 19). In Fig. 18 it is manifested by the 'stepped'

form of the pressure distribution (*see*, for example, the curve for $i p_2/p_1 = 3.51$). With increasing jet pressure the separation point moves downstream until when $i p_2/p_1 = 6$ (approx.) the initial shock reaches the nozzle exit plane. (Fig. 18 shows that, because of the 'smoothing' tendency of the boundary layer on strong pressure gradients, the surface pressure starts to increase slightly upstream of the exit plane.) At this point $M_2 = 2.0$ but p_2 is less than p_1 . Thereafter the nozzle runs full (no internal separation) so that M_2 and $p_2/i p_2$ are constant. Consequently, as $i p_2/p_1$ increases p_2 increases also and the shock weakens (*see* Figs. 18 and 19) until, when $i p_2/p_1 = 7$ (approx.), $p_2 = p_1$ and the flow is discharged parallel to the axis. A further increase in $i p_2/p_1$ causes p_2 to rise above p_1 (under-expansion) and an expansion fan forms at the nozzle lip. Because of the axial symmetry of the flow this fan is followed by a shock, which is weak near the nozzle lip, but which strengthens downstream. In meridian section, the upper and lower branches of this shock intersect at a point on the axis (regular intersection) provided that $i p_2/p_1 < 14$ (approx.). When, however, $i p_2/p_1 > 14$ a normal shock is formed before the apex is reached (Mach intersection) and a vortex sheet extends downstream of the triple intersection point. This sequence is clearly shown by the schlieren photographs in Fig. 19.

A further point concerning Fig. 18 may be mentioned here. The curves indicate that when separation occurs inside the nozzle and close to the lip, the pressure ratio across the initial shock at the separation point is about 1.2. This value, moreover, was confirmed by the results obtained with four other supersonic nozzles (Models 2-5-40 (60) (80) and 2-10-60). It is, however, considerably less than the value of 2.0 measured by Beastall and Eggink¹ (at the same Mach number and with a turbulent boundary layer) in experiments on shock-induced separation with a two-dimensional step. The reason for this discrepancy is not certain but it may result from interference caused by reflections of the primary shock.

Comparison of Figs. 8 and 18 shows that the surface pressure distribution inside the nozzle at a given value of $i p_2/p_B$ with external flow is practically identical with the pressure distribution at the same value of $i p_2/p_1$ without external flow. Upstream propagation through the mixing region of disturbances in the field of the external jet does not, therefore, appreciably affect the distribution of pressure on the nozzle walls.

Schlieren photographs illustrating the effect of pressure ratio on the structure of the jet from a sonic nozzle (1-0-60) are shown in Fig. 20. These photographs are presented in pairs, one member of each pair being taken with a vertical knife-edge (to emphasise the axial density gradient) and the other with a horizontal knife-edge (to emphasise the radial density gradient). Comparing the latter with the corresponding photographs shown in Fig. 19 for a supersonic nozzle (2-0-60) we observe that, when the flow is under-expanded, the two jets develop with pressure ratio in much the same manner. It is to be noted however that, with a sonic nozzle, when $i p_2/p_1$ is decreased below the critical value corresponding to $p_2 = p_1$ and $M_2 = 1$, the flow becomes subsonic throughout the nozzle. Consequently, over-expansion ($p_2 < p_1$) accompanied by internal separation cannot occur.

5.2. *The Data on Jet Thrust.* We define the jet thrust (S) by the equation:

$$S = Q u_2 + (p_2 - p_1) a_2. \quad (5)$$

With this definition, assuming that:

- (1) The flow is one-dimensional and isentropic.
- (2) The velocity is sonic in the nozzle throat.
- (3) The flow does not separate inside the nozzle,

it is easily shown that:

$$\frac{S}{a_0 p_1} = f(\gamma, M_2^*) \frac{i p_2}{p_1} - g(\gamma, M_2^*) \quad (6)$$

where

$$f(\gamma, M_2^*) = \gamma \sqrt{\left(\frac{\gamma+1}{2}\right) \left(\frac{2}{\gamma+1}\right)^{\frac{\gamma}{\gamma-1}}} \frac{M_2^*}{\sqrt{\left\{1 + \left(\frac{\gamma-1}{2}\right) (M_2^*)^2\right\}}} + \frac{i p_2 a_2}{i p_2 a_0}$$

and

$$g(\gamma, M_2^*) = \frac{a_2}{a_0}.$$

On these assumptions, therefore, the graph of $S/a_0 p_1$ against $i p_2/p_1$ for a given nozzle is a straight line whose gradient and intercept depend on γ and the nozzle design Mach number (M_2^*).

In Fig. 21 the experimental values of $S/a_0 p_1$ (obtained from the balance readings) are plotted against $i p_2/p_1$ for four supersonic nozzles ($M_2^* = 2.0$) and a sonic nozzle ($M_2^* = 1.0$). Superimposed on these results are the corresponding theoretical curves for $M_2^* = 2.0$ and $M_2^* = 1.0$. These latter were calculated from Equation (6) above, taking $\gamma = 1.4$. We note that the experimental points for the four supersonic nozzles lie approximately on the same straight line, but the gradient of this line is slightly less than that predicted theoretically. In the case of the sonic nozzle also, $S/a_0 p_1$ increases linearly with $i p_2/p_1$ at slightly less than the theoretical rate.

This loss in thrust is attributed mainly to the boundary layer, which tends to reduce the mass flow through the nozzle, and also creates drag due to skin friction. As the results obtained with model 2-5-60 ($\beta_2 = 5$ deg) lie on the same straight line as those obtained with model 2-0-60 ($\beta_2 = 0$ deg), we may infer that the finite radial exit momentum in the former case has no appreciable effect on the thrust.

In the above analysis, the measured thrust produced by a given nozzle operating at a given pressure ratio, is compared with the theoretical thrust produced by the same nozzle, operating at the same pressure ratio, assuming one-dimensional isentropic flow. It is also instructive to compare both these quantities with the 'ideal' thrust (\bar{S}). \bar{S} is defined as the thrust produced by a nozzle (assuming one-dimensional isentropic flow) which:

- (1) Has the same throat area (a_0).
- (2) Operates at the same pressure ratio ($i p_2/p_1$).
- (3) Discharges the working fluid at the ambient static pressure ($p_2 = p_1$).

It is the maximum thrust physically obtainable by expanding a given mass flow through a given pressure ratio and, for this reason, forms a useful basis for comparison. It is easily shown that:

$$\frac{\bar{S}}{a_0 p_1} = \frac{2\gamma}{\gamma-1} \sqrt{\left(\frac{\gamma-1}{\gamma+1}\right) \left(\frac{2}{\gamma+1}\right)^{\frac{1}{\gamma-1}}} \frac{i p_2}{p_1} \sqrt{\left\{1 - \left(\frac{p_1}{i p_2}\right)^{\frac{\gamma-1}{\gamma}}\right\}}. \quad (7)$$

In Fig. 22 the experimental values of the thrust efficiency (S/\bar{S}) are plotted against $i p_2/p_1$ for the five nozzles previously considered in Fig. 21. Also shown are the theoretical values for $M_2^* = 2.0$ and $M_2^* = 1.0$ [S calculated from Equation (6)]. We consider first the theoretical curve for $M_2^* = 2.0$. When $i p_2/p_1 = 7.8$, $p_2 = p_1$ and S/\bar{S} is, by definition, equal to unity. When $i p_2/p_1 > 7.8$, $p_2 > p_1$ (under-expansion) and the thrust could be increased by increasing the nozzle area ratio (a_2/a_0). Hence the thrust (S) is less than the maximum physically obtainable (\bar{S}), so that $S/\bar{S} < 1$.

Conversely, when $i p_2/p_1 < 7.8$, $p_2 < p_1$ (over-expansion) and the thrust could be increased by decreasing a_2/a_0 so that, by the same reasoning, $S/\bar{S} < 1$. Similar remarks apply to the theoretical curve for the sonic nozzle with under-expanded flow.

The experimental curves for the supersonic nozzles, which agree quite closely at the higher pressure ratios, tend to diverge as the pressure ratio is decreased. This spread (which is not apparent on the scale of Fig. 21) may be due, at least in part, to small experimental errors in the measurement of S , which are accentuated by the method of plotting. (When $i p_2/p_1$ is small, \bar{S} is also small, and a small absolute zero error in S gives rise to a large error in S/\bar{S} .) It will, however, be apparent that although the readings may be slightly in error when $i p_2/p_1$ is small, the experimental curves for both the supersonic and sonic nozzles are similar in shape to the corresponding theoretical curves, but lie slightly below them. The reason for this lies in the boundary-layer effect mentioned previously in connection with Fig. 21.

Fig. 22 also illustrates a practical point in connection with the design of a convergent-divergent nozzle for a supersonic aircraft. It is apparent that over-expansion causes the thrust to decrease more rapidly than under-expansion. By choosing the nozzle area-ratio (a_2/a_0) to give slight under-expansion at the cruising speed we may, therefore, substantially improve the low speed thrust at the cost of a relatively small decrease in the cruising thrust.

6. *The Correlation of the Base Pressure Data.* A method of correlating data on annular base pressures has been proposed and discussed briefly in Section 1. In this section we will restate the underlying ideas and examine the experimental evidence in detail.

The essential basis of the method lies in comparing the pressure on an annular base with the calculated pressure on the 'corresponding' two-dimensional base. In this context, 'corresponding' means that the two profiles are congruent in section, and that M_1 , M_2 and $i p_2/i p_1$ (see Fig. 2) are identical in the two cases.

The method used to calculate two-dimensional base pressures depends on the 'critical' pressure rise concept first stated explicitly by Beastall and Eggink¹. It is not necessary to enter into details here (see, for example, Ref. 2) except to point out that, with three restrictions, the method is applicable to the most general two-dimensional problem in which a base separates two streams, inclined to one another, and of different Mach number and total pressure. The restrictions are:

- (1) We consider only Phase 3 of the base pressure curve (see Section 4.1.1).
- (2) We assume that the boundary layers are turbulent and thin compared with the base height.
- (3) We assume that there is no interference between the two halves of the base flow. This implies that the jet Mach number (M_2) must be greater than unity.

Subject to these restrictions, if we define:

$$(p_B/p_1)_2^3 = (p_B/p_1)_3/(p_B/p_1)_2$$

where $(p_B/p_1)_3$ refers to the annular base

and $(p_B/p_1)_2$ refers to the corresponding two-dimensional base then we may write:

$$(p_B/p_1)_2^3 = F\left(M_1, M_2, \beta_1, \beta_2, \frac{d_2}{d_1}, \frac{i p_2}{i p_1}\right). \quad (8)$$

Now it is clear, on geometrical grounds, that as

$$\frac{d_2}{d_1} \rightarrow 1, (p_B/p_1)_3 \rightarrow (p_B/p_1)_2 \text{ so that } (p_B/p_1)_2^3 \rightarrow 1.$$

Hence $(p_B/p_1)_2^3$ is independent of M_1 , M_2 , β_1 , β_2 and $i p_2/i p_1$ when $d_2/d_1 = 1$ and might reasonably be expected to be insensitive to these five variables provided that d_2/d_1 is not too far removed from unity. Graphically, this is equivalent to saying that when $(p_B/p_1)_2^3$ is plotted against d_2/d_1 all the points may be expected to lie on, or close to, a curve through the point (1, 1). If such a unique correlation curve exists, to a sufficient degree of approximation, the solution of an annular base pressure problem is immediately reduced to the known solution of the corresponding problem in two dimensions.

We turn now to the experimental evidence, and replot the data presented in Figs. 9, 11 and 13 in a more appropriate form. Fig. 23 shows $(p_B/p_1)_2^3$ plotted against $i p_2/i p_1$ for the six supersonic nozzles. (The results for the sonic nozzle are omitted in accordance with condition (3) above.) It is immediately apparent that $(p_B/p_1)_2^3$ is largely independent of $i p_2/i p_1$, and this is true even when d_2/d_1 is quite small ($d_2/d_1 = 0.4$). To this extent at least, therefore, the provisional reasoning given above is borne out by experiment.

The form of the correlation curve is shown by Fig. 24, in which $(p_B/p_1)_2^3$ is plotted against d_2/d_1 for the supersonic nozzles. In this graph the spread in $(p_B/p_1)_2^3$ with $i p_2/i p_1$ for each model is indicated by a full vertical line. We note, firstly, that the results for $\beta_2 = 5$ deg lie approximately on a smooth curve* which passes, as it should, through the point (1, 1). The correlation with β_2 is not so good, but is probably sufficiently close for most practical purposes. The present data do not suffice to test the effect of M_1 , M_2 and β_1 as these variables were maintained constant throughout the experiment. To sum up, we may fairly conclude that the proposed method correlates the present results tolerably well, but these results are insufficient to afford a comprehensive test.

In these circumstances it is natural to widen the scope by including the results of other workers³. When this is done we find that a substantial body of these results fits the correlation curve shown in Fig. 24. There remains, however, an anomalous residue (chiefly at the higher Mach numbers) which are widely scattered. This scatter may be due to:

- (1) Failure of the correlation method.
- (2) Failure of the method used to calculate two-dimensional base pressures.
- (3) Errors in the experimental data.

There is some evidence to indicate that the method used to calculate two-dimensional base pressures under-estimates the base pressure at high Mach numbers. There is also evidence that at least some of the anomalous experimental results are incorrect, in that they are not self-consistent. The position is, in fact, rather confusing as yet, and much remains to be done. Further analysis is planned, supplemented, if necessary, by experimental work.

7. Conclusions. The more important results presented in the main body of the Report, and the conclusions drawn from them, are summarised below:

(a) Tests with external flow. Base pressure data

(1) The effect of jet pressure ratio ($i p_2/i p_1$) on base pressure (p_B/p_1) falls naturally into three phases. (Section 4.1.1 and Fig. 5.) As $i p_2/i p_1$ is increased p_B/p_1 first rises (Phase 1), and then drops rapidly (Phase 2) until it is considerably less than the value corresponding to a sealed base. Thereafter, p_B/p_1 increases steadily with $i p_2/i p_1$ (Phase 3). These three phases, which were observed with each of the seven models tested, correspond to fundamental differences in the physical nature of the base flow.

* This correlation curve is actually a straight line, but this does not appear to be significant.

(2) At a given value of p_2/p_1 in Phase 3, p_B/p_1 increases with increase in the jet/base diameter ratio (d_2/d_1), decreases with increase in nozzle design Mach number (M_2^*), and increases with increase in nozzle divergence angle (β_2) (Figs. 9, 11 and 13 respectively).

(3) A method of correlating data on annular base pressures is proposed (Section 6). The essential principle of this method is to compare the measured pressure on the annular base with the calculated pressure on the corresponding two-dimensional base. The method correlates the present data reasonably well (Fig. 24), but is less successful when the results of others are included.

(b) Tests with external flow. Thrust and drag data

(4) Provided that there is no separation within the nozzle, the jet thrust coefficient $[(C_T)_{\text{jet}}]$ at a given value of p_2/p_1 is the same either with or without external flow. Consequently, the overall thrust coefficient in supersonic flight $[(C_T)_{\text{jet}} - (C_D)_{\text{base}}]$ may be calculated accurately from force measurements without external flow coupled with base pressure measurements with external flow.

(5) Comparison of the force measurements on a supersonic nozzle ($M_2^* = 2.0$) and a sonic nozzle ($M_2^* = 1.0$) with the same throat/base diameter ratio ($d_0/d_1 = 0.6$) shows that the overall thrust coefficient of the former exceeds that of the latter at all but the lowest values of jet pressure ratio (Fig. 15).

(6) Force measurements on three supersonic nozzles ($M_2^* = 2.0$, $d_2/d_1 = 0.6$) show that the overall thrust coefficient is independent of nozzle divergence angle (β_2) in the range $0 < \beta_2 < 10$ deg (Fig. 16).

(c) Tests with external flow. Base bleed data

(7) When air is progressively introduced into the 'dead' region behind a sealed base, the base pressure first rises and then drops. (Section 4.3.) The two primary parameters are the non-dimensional bleed mass flow (or 'bleed number' H) and the ratio bleed duct diameter/base diameter (d_2/d_1).

(8) Provided that H is small, p_B/p_1 increases linearly with H and is independent of d_2/d_1 , but when H is not small p_B/p_1 increases with d_2/d_1 for constant H (Fig. 17).

(9) The combined drag of the base and bleed duct (discounting any intake drag) is least when the correct quantity of air is discharged through a duct with the largest possible exit diameter. (Table 2, Section 4.3.) This conclusion may be subject to qualification when the intake drag of the bleed air is taken into account.

(d) Tests without external flow. Thrust data

(10) With both the supersonic and sonic nozzles, the measured values of the non-dimensional thrust ($S/a_0 p_1$) increase linearly with p_2/p_1 at a rate which is slightly less than that predicted by one-dimensional isentropic theory (Fig. 21). This loss in thrust is attributed to the boundary layer, which decreases the mass flow through the nozzles and also creates skin-friction drag.

(11) When the measured thrust (S) is compared with \bar{S} (corresponding to one-dimensional isentropic expansion down to the ambient static pressure), the maximum value of S/\bar{S} is 0.93 for the sonic nozzle and lies between 0.95 and 0.99 for the supersonic nozzles. With the supersonic nozzles S/\bar{S} decreases slowly with under-expansion, but more rapidly with over-expansion (Fig. 22).

LIST OF SYMBOLS

$()_0$, $()_1$ and $()_2$	Refer to the positions shown in Fig. 2
$()_B$	Denotes an average value over the base annulus
$()_i$	Denotes stagnation conditions
$()^*$	Indicates a design value based on one-dimensional isentropic flow. (When applied to a flow parameter)

Flow parameters

M	Mach number
ρ	Density
p	Static pressure
T	Static temperature
u	Velocity
Q	Mass flow through central nozzle
γ	Ratio of specific heats
R	Gas constant
$q =$	$\frac{1}{2}\rho u^2$

Geometrical parameters

d	Diameter
a	Area
β	Angle between tangent to surface and axis in meridian plane
l	Axial position of base relative to a suitable reference plane of the tunnel nozzle

Boundary-layer parameters

δ^*	Displacement thickness
θ	Momentum thickness

Bleed parameter

H	Bleed number, defined by $H = \sqrt{\left(\frac{R}{\gamma}\right) \frac{Q\sqrt{i}T_1}{a_{1i}p_1}}$
-----	--

Thrust and drag coefficients

$(C_T)_{\text{jet}}$	Jet thrust coefficient, defined by Equation (3)
$(C_D)_{\text{base}}$	Base drag coefficient, defined by Equation (4)
S	Jet thrust, defined by Equation (5)
\bar{S}	'Ideal' jet thrust, defined by Equation (7)

Miscellaneous symbols

$(p_B/p_1)_2$, $(p_B/p_1)_3$ and $(p_B/p_1)_2^3$ are defined in Section 6

REFERENCES

- | <i>No.</i> | <i>Author</i> | <i>Title, etc.</i> |
|------------|---|--|
| 1 | D. Beastall and H. Eggink .. | Some experiments on breakaway in supersonic flow (Part II).
Unpublished M.O.A. Report. |
| 2 | E. M. Cortright | Some aerodynamic considerations of nozzle-afterbody combinations.
<i>Aero. Eng. Rev.</i> Vol. 15. No. 9. 1956. |
| 3 | A. F. Bromm, Jr. and
R. M. O'Donnell | Investigation at supersonic speeds of the effect of jet Mach number
and divergence angle of the nozzle upon the pressure of the base
annulus of a body of revolution.
N.A.C.A. Research Memo. L54I16. TIL 4521. December, 1954. |
| 4 | J. Reid and R. C. Hastings .. | Experiments on the axisymmetric flow over afterbodies and bases
at $M = 2.0$.
A.R.C. 21,707. October, 1959. |
| 5 | L. Fuller and J. Reid | Experiments on two-dimensional base flow at $M = 2.4$.
A.R.C. R. & M. No. 3064. February, 1956. |
| 6 | H. H. Korst, R. H. Page and
M. E. Childs | A theory for base pressures in transonic and supersonic flow.
University of Illinois. Engineering Experiment Station. Mech. Eng.
Dept. ME Tech. Note 392-2. March, 1955. |

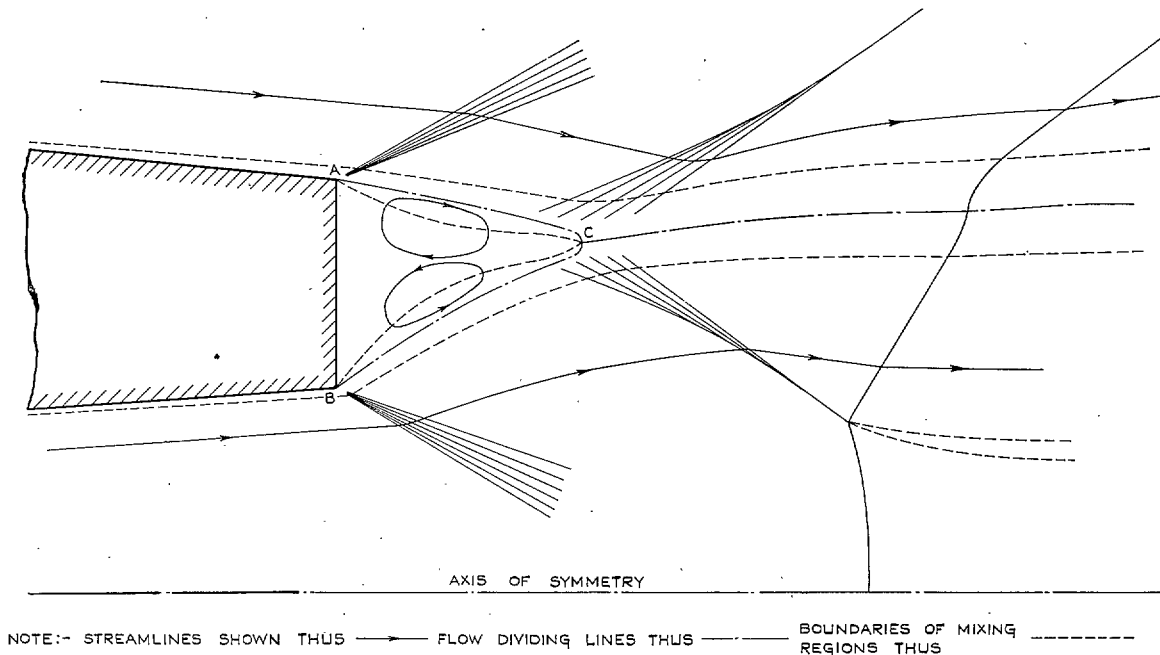


FIG. 1. Schematic diagram showing flow field behind annular base.

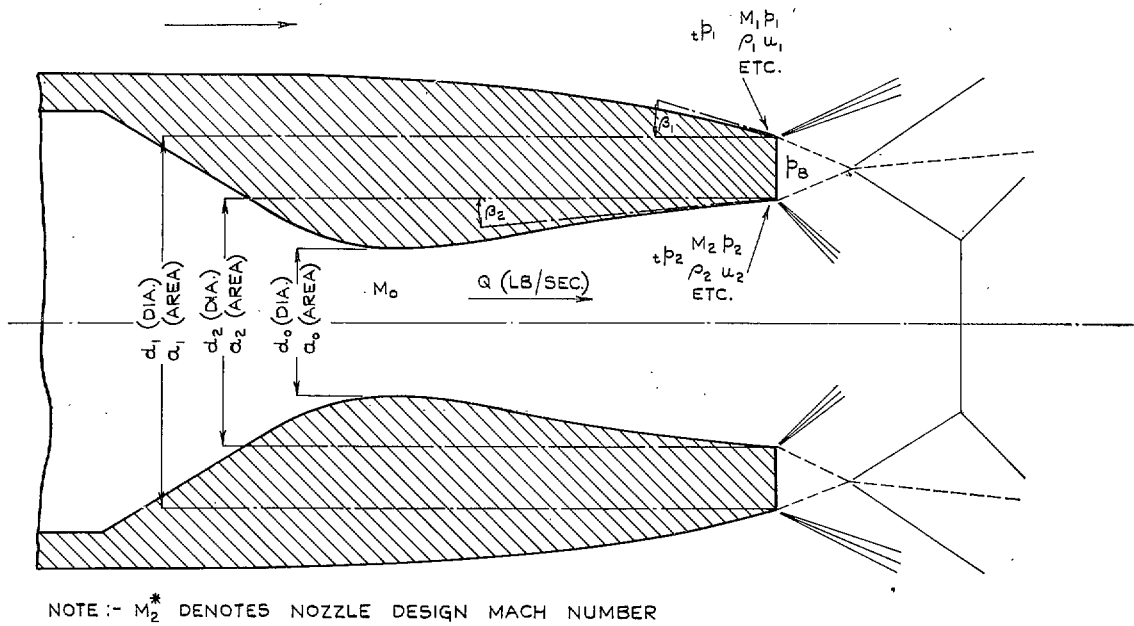


FIG. 2. Diagram showing notation used in report.

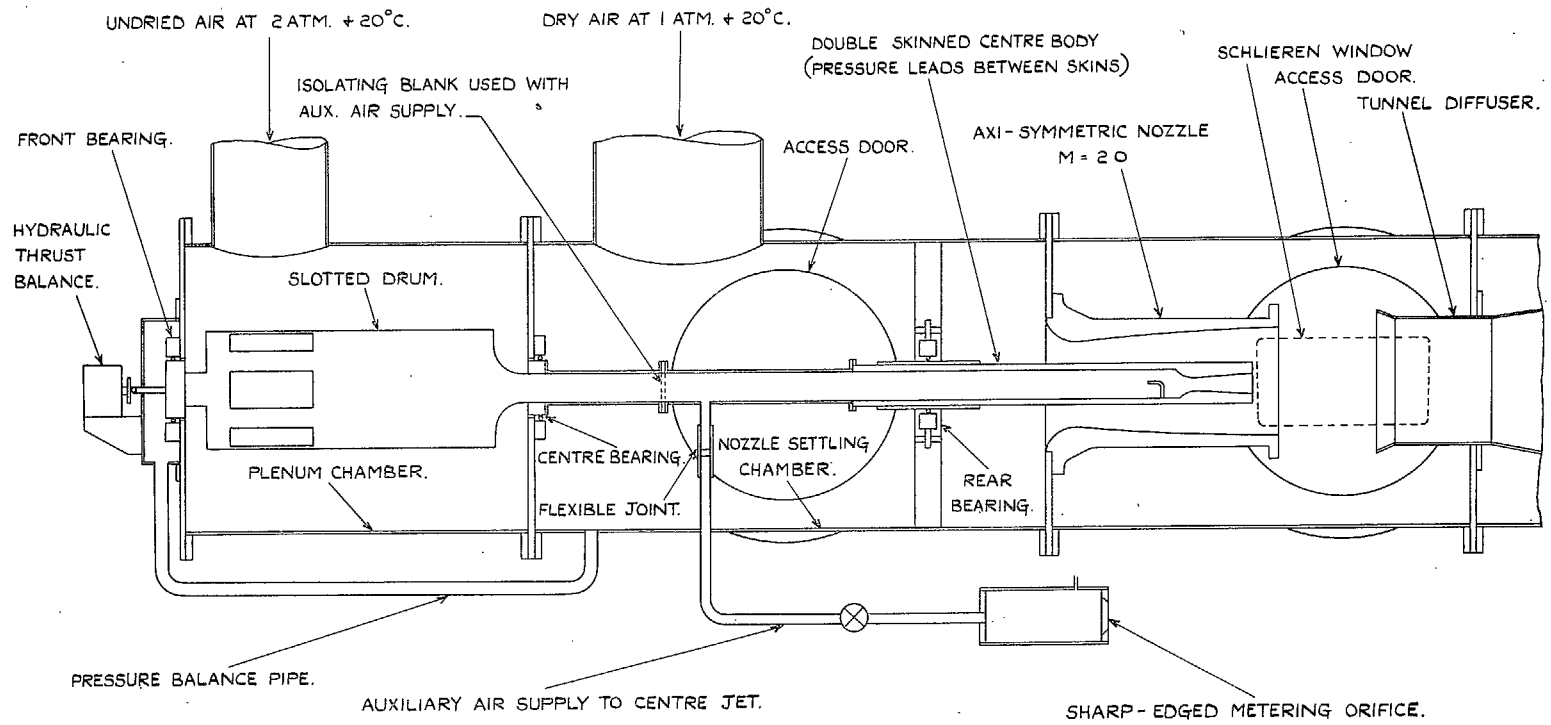
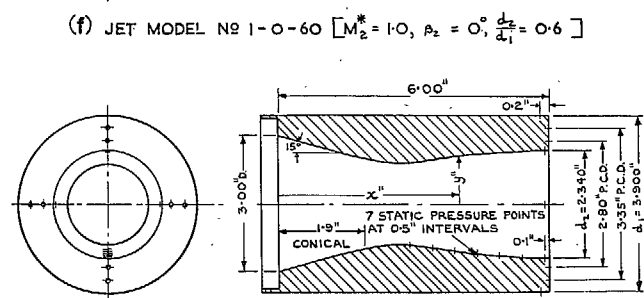
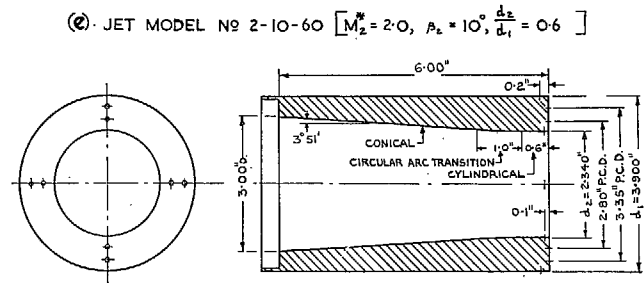
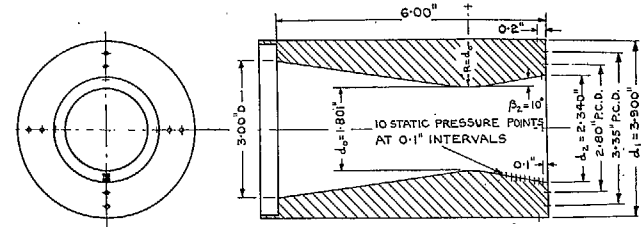
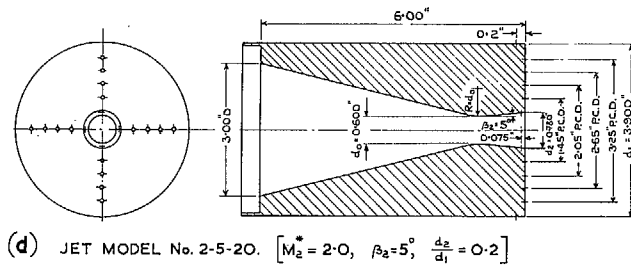
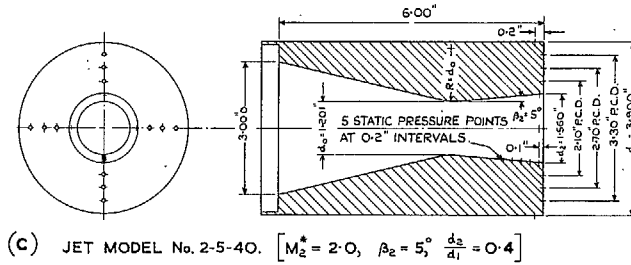
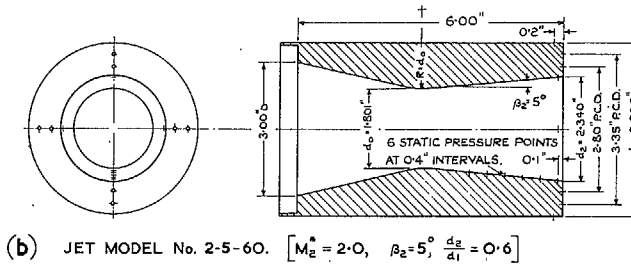
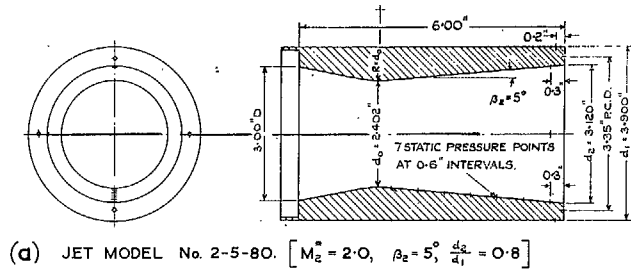


FIG. 3. Supersonic tunnel (No. 16) for tests on jet interference.



NOZZLE CO-ORDINATES

x (IN.)	1.9	2.1	2.3	2.5	2.7	2.9	3.1	3.3	3.5
y (IN.)	1.0080	0.9565	0.9165	0.8770	0.8375	0.7980	0.7585	0.7190	0.6795
z (IN.)	3.7	3.9	4.1	4.3	4.5	4.7	4.9	5.1	5.3
y (IN.)	1.0430	1.0665	1.0875	1.1060	1.1355	1.1550	1.1660	1.1700	1.1700

FIG. 4 (a to g). Jet models. Leading dimensions and positions of static pressure points.

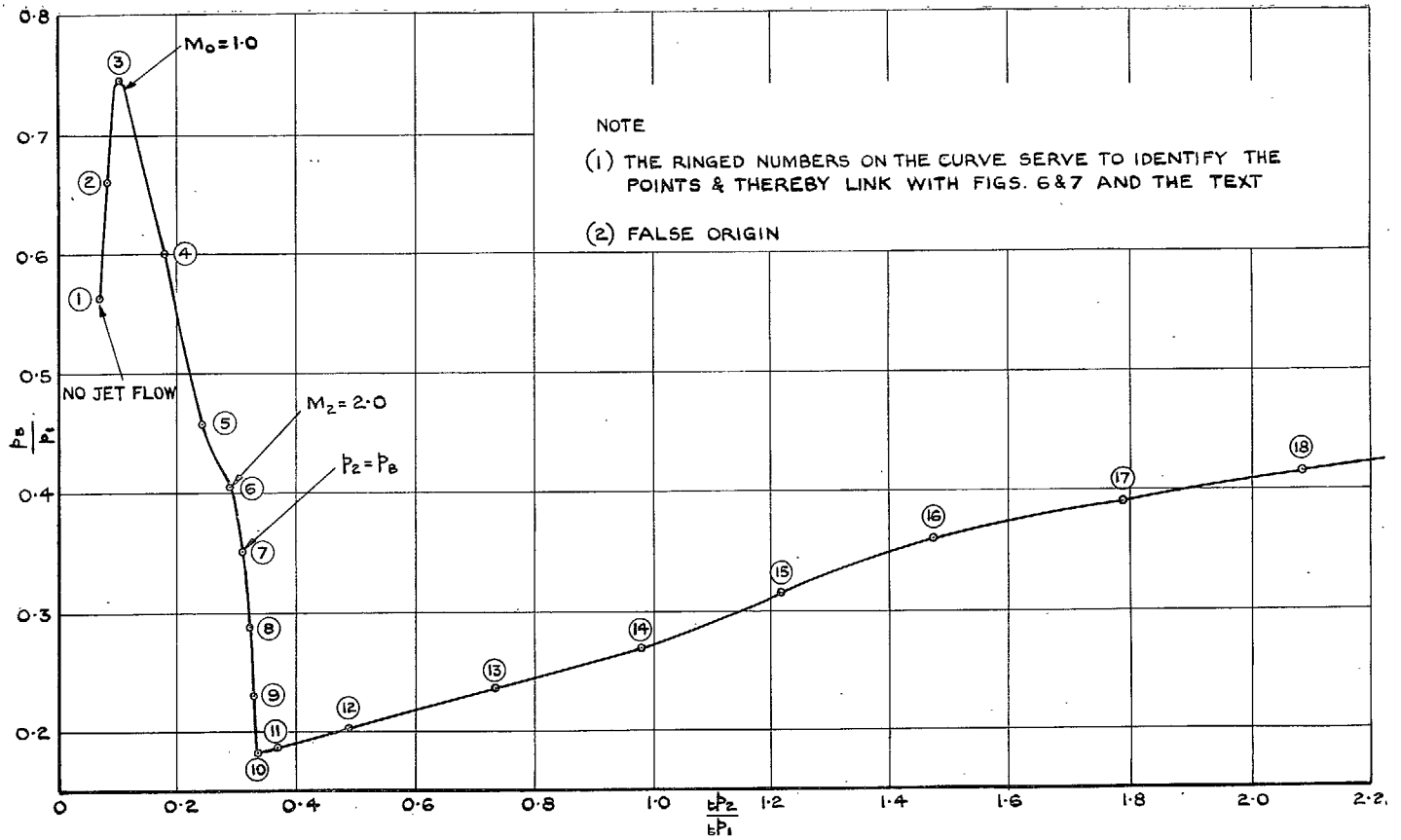


FIG. 5. The effect of jet pressure ratio on base pressure. Model No. 2-0-60.

[$M_1 = 2.0$, $M_2^* = 2.0$, $\beta_1 = 0$ deg, $\beta_2 = 0$ deg, $d_2/d_1 = 0.6$.]

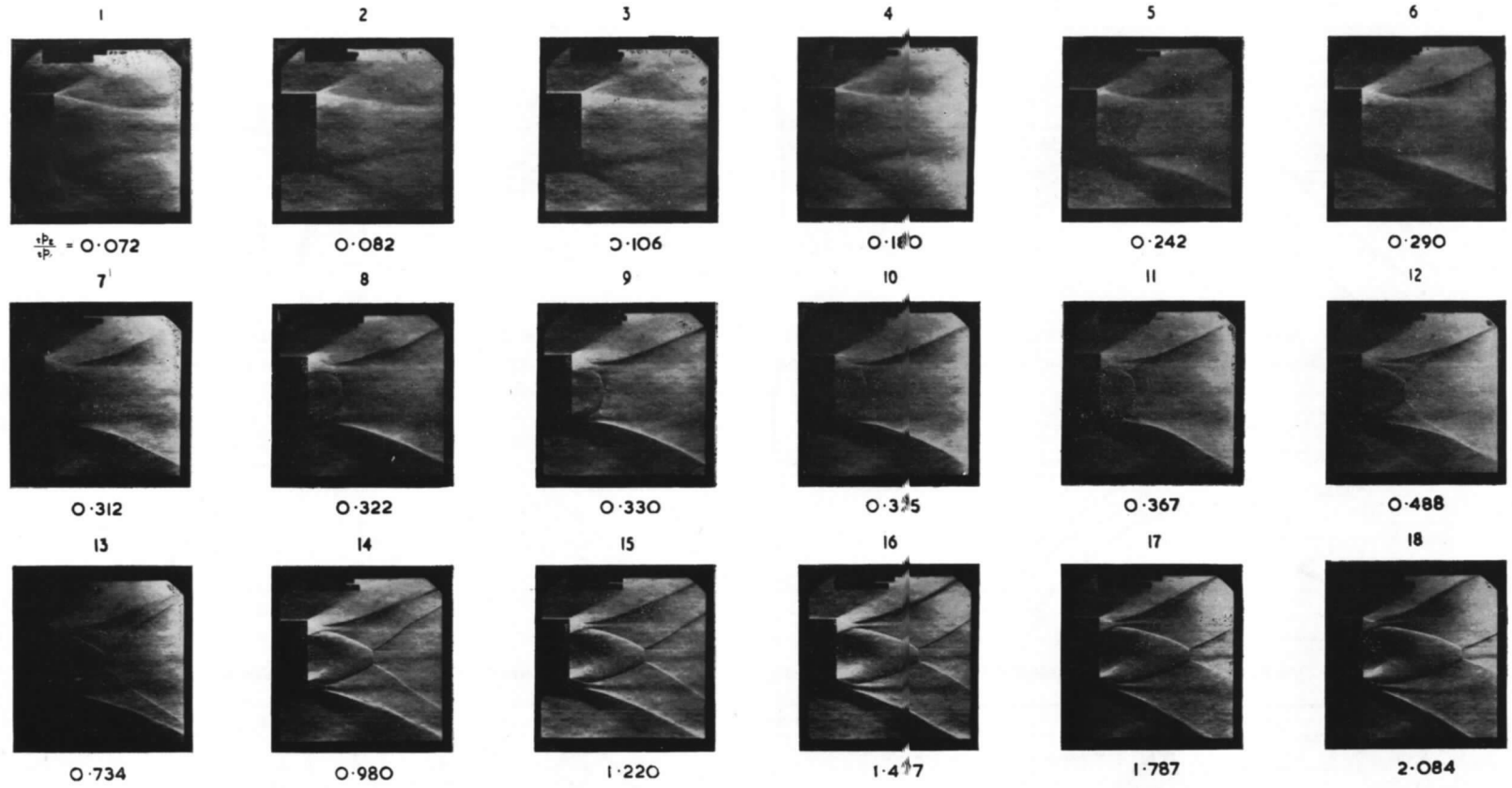
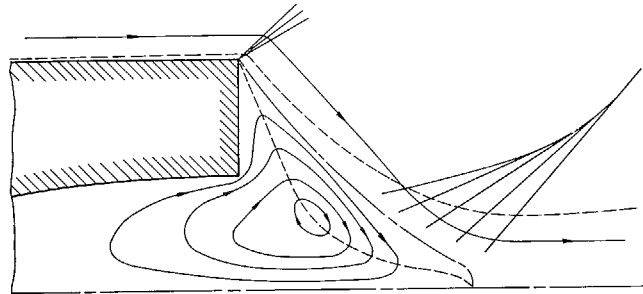
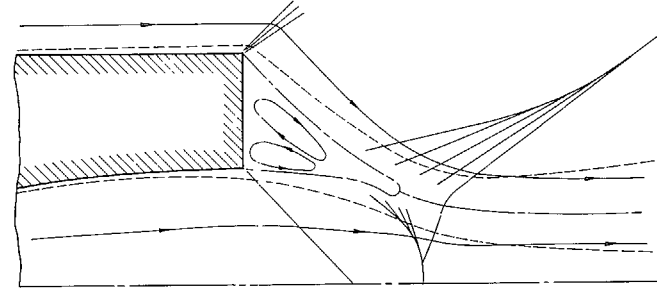


FIG. 6. Schlieren photographs showing the effect of jet pressure ratio on the base flow. Model No. 2-0-60.

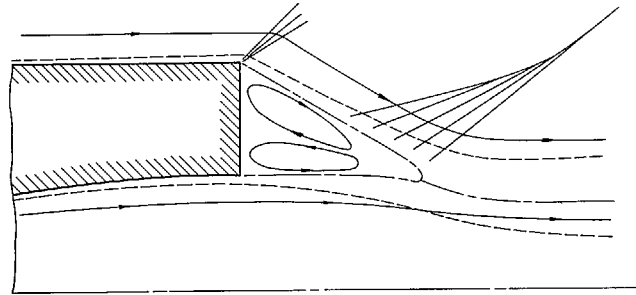
$[M_1 = 2.0, M_2^* = 2.0, \beta_1 = 0 \text{ deg}, \beta_2 = 0 \text{ deg}, d_2/d_1 = 0.6.]$



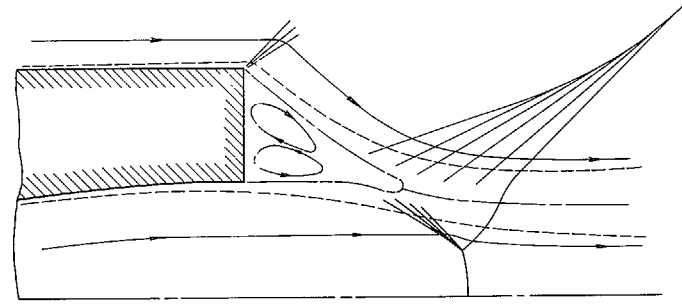
(a). FLOW FIELD CORRESPONDING TO POINT ① IN FIG. 5.



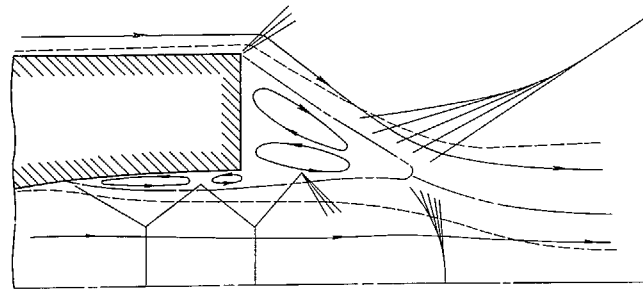
(d). FLOW FIELD CORRESPONDING TO POINT ⑥ IN FIG. 5.



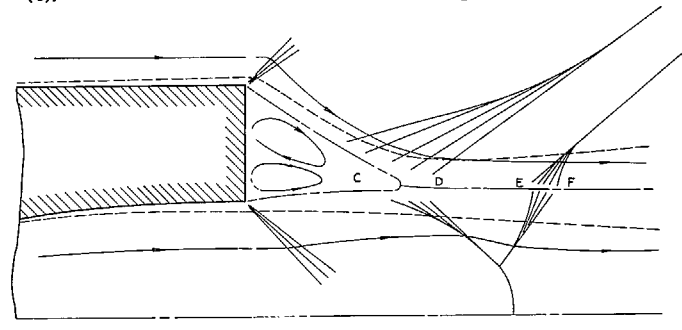
(b). FLOW FIELD CORRESPONDING TO POINT ③ IN FIG. 5.



(e). FLOW FIELD CORRESPONDING TO POINT ⑦ IN FIG. 5.



(c). FLOW FIELD CORRESPONDING TO POINT ④ IN FIG. 5.



(f). FLOW FIELD CORRESPONDING TO POINT ⑫ IN FIG. 5.


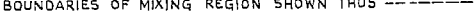
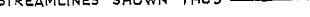
NOTE : FLOW DIVIDING LINES SHOWN THUS  BOUNDARIES OF MIXING REGION SHOWN THUS  STREAMLINES SHOWN THUS 

FIG. 7 (a to f). Schematic diagrams showing effect of jet pressure ratio on base flow.

NOTE: (1) \odot DENOTES BASE PRESSURE READING

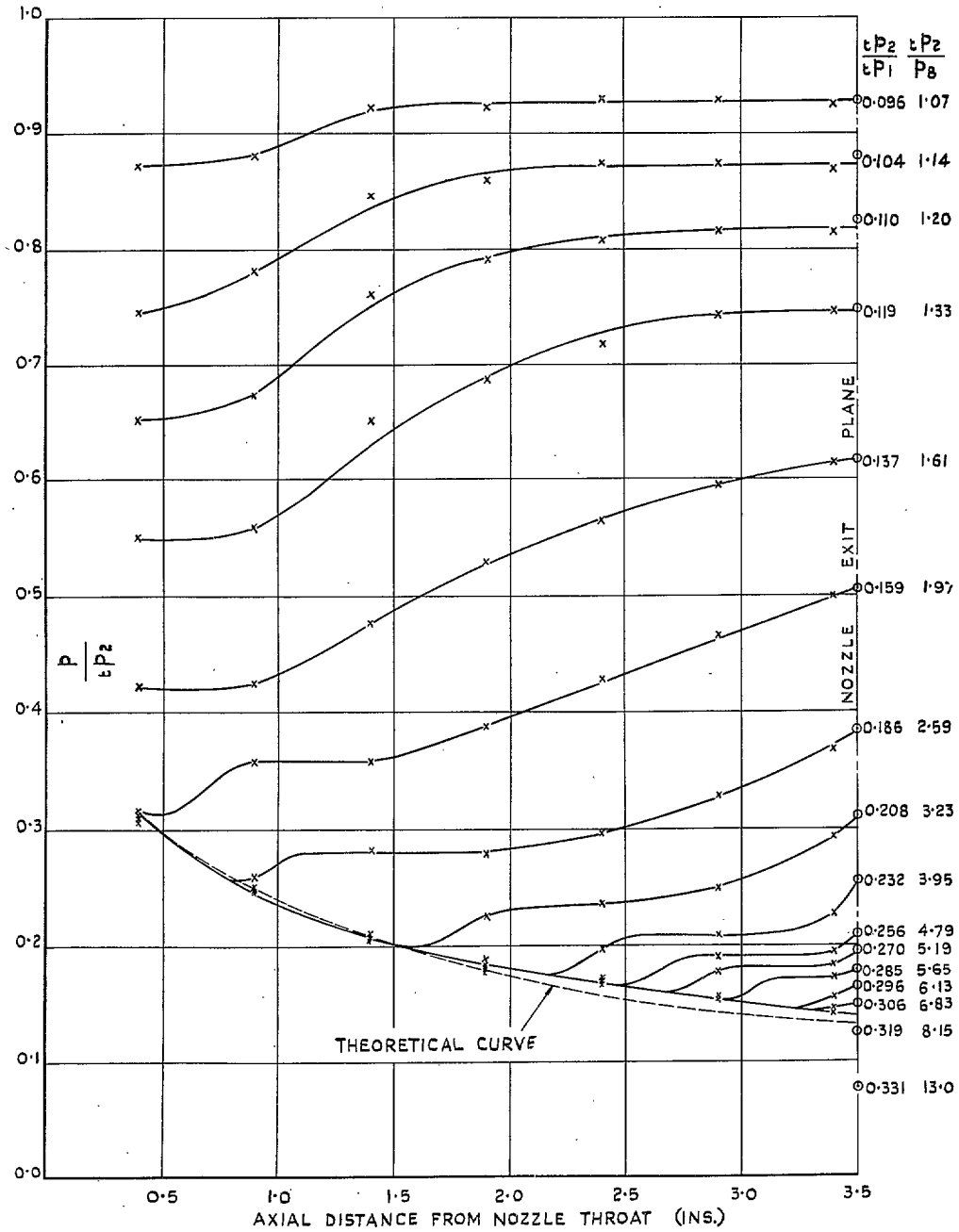


FIG. 8. The effect of jet pressure ratio on the pressure distribution inside the nozzle. Model No. 2-0-60.

$$[M_1 = 2.0, M_2^* = 2.0, \beta_1 = 0 \text{ deg}, \beta_2 = 0 \text{ deg}, d_2/d_1 = 0.6.]$$

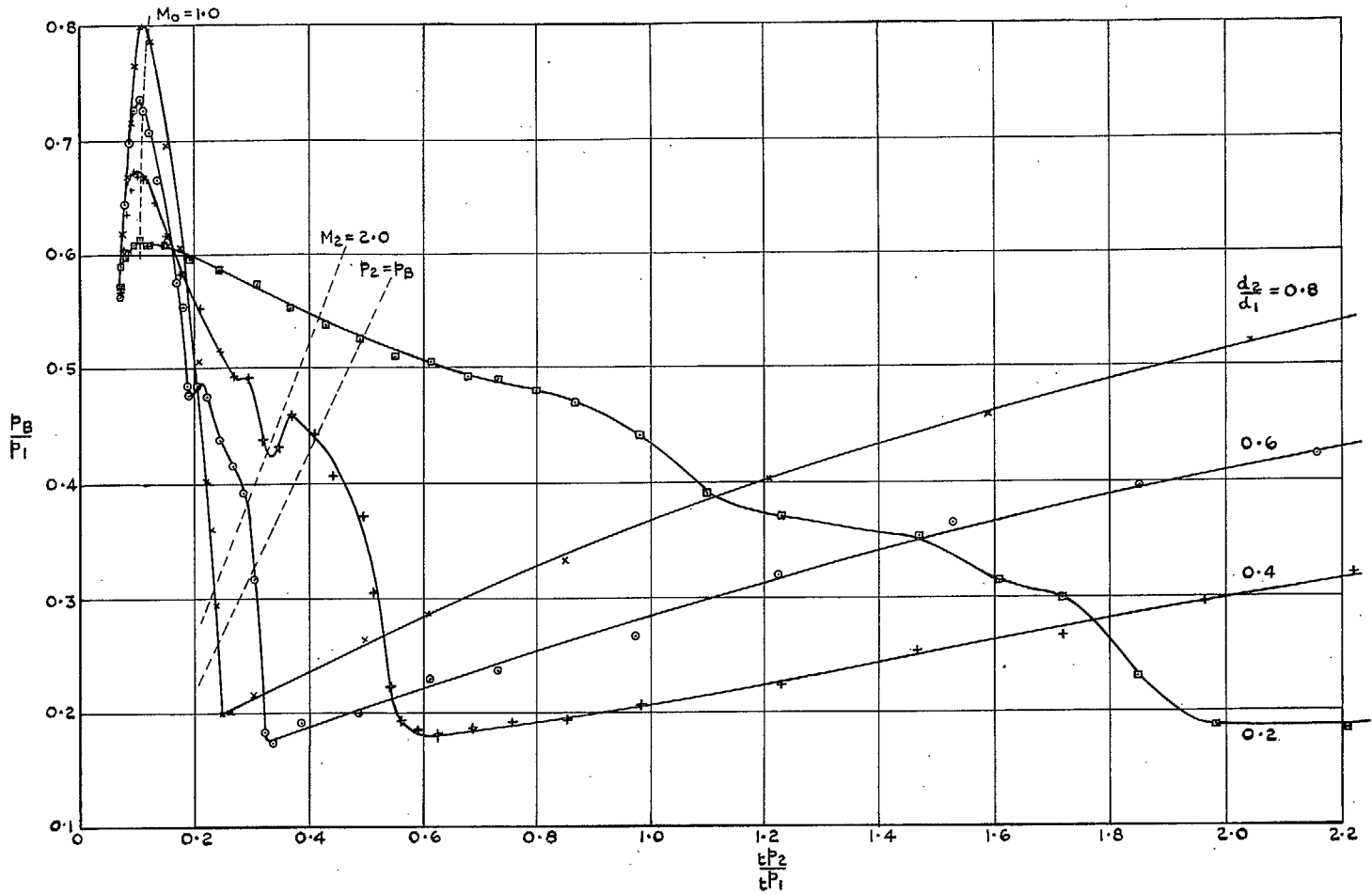
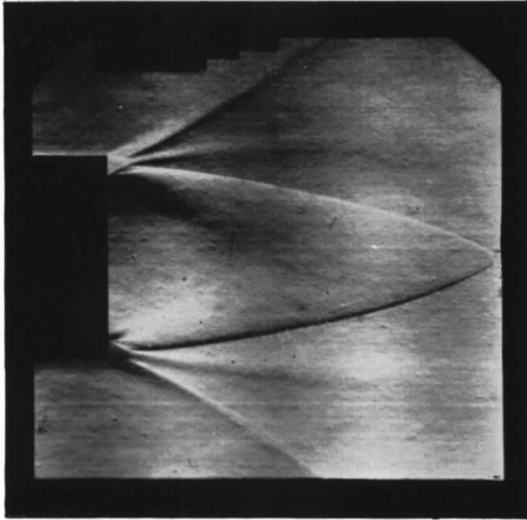
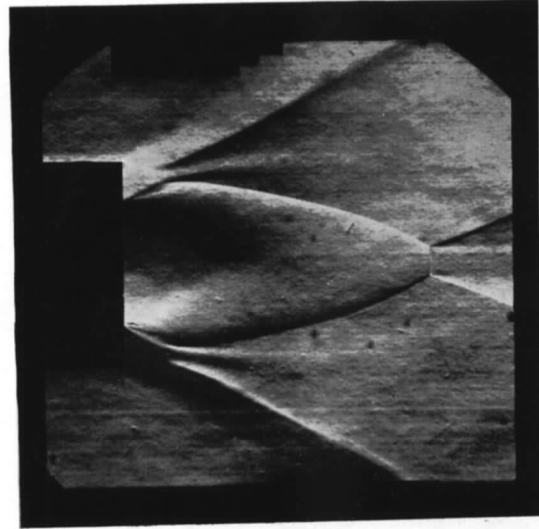


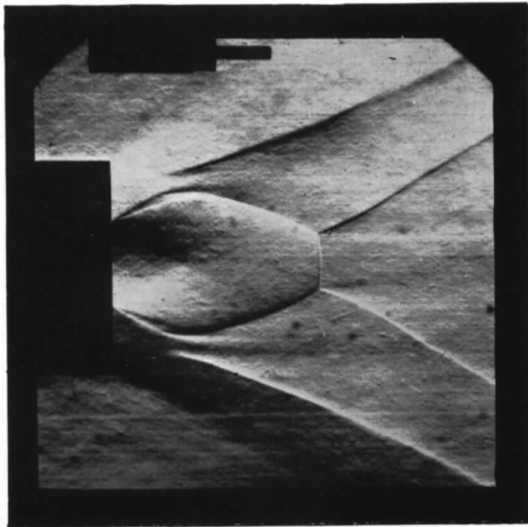
FIG. 9. The effect of jet/base diameter ratio on base pressure.
 [$M_1 = 2.0$, $M_2^* = 2.0$, $\beta_1 = 0$ deg, $\beta_2 = 5$ deg.]



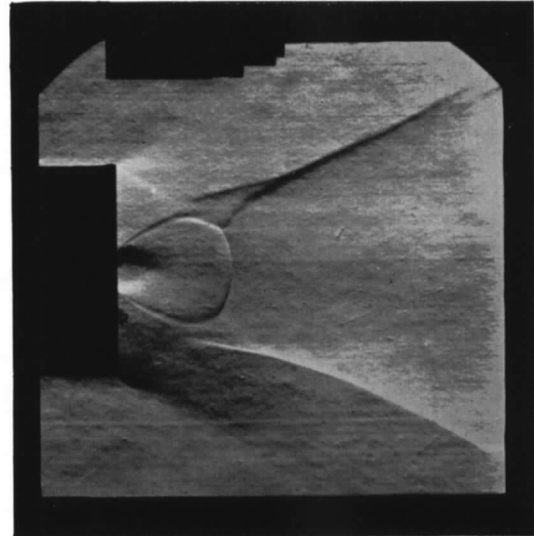
$$\frac{d_2}{d_1} = 0.8$$



$$\frac{d_2}{d_1} = 0.6$$



$$\frac{d_2}{d_1} = 0.4$$



$$\frac{d_2}{d_1} = 0.2$$

FIG. 10. Schlieren photographs showing the effect of jet/base diameter ratio on the base flow.
[$M_1 = 2.0$, $M_2^* = 2.0$, $\beta_1 = 0$ deg, $\beta_2 = 5$ deg, $t_{p_2}/t_{p_1} = 2.35$.]

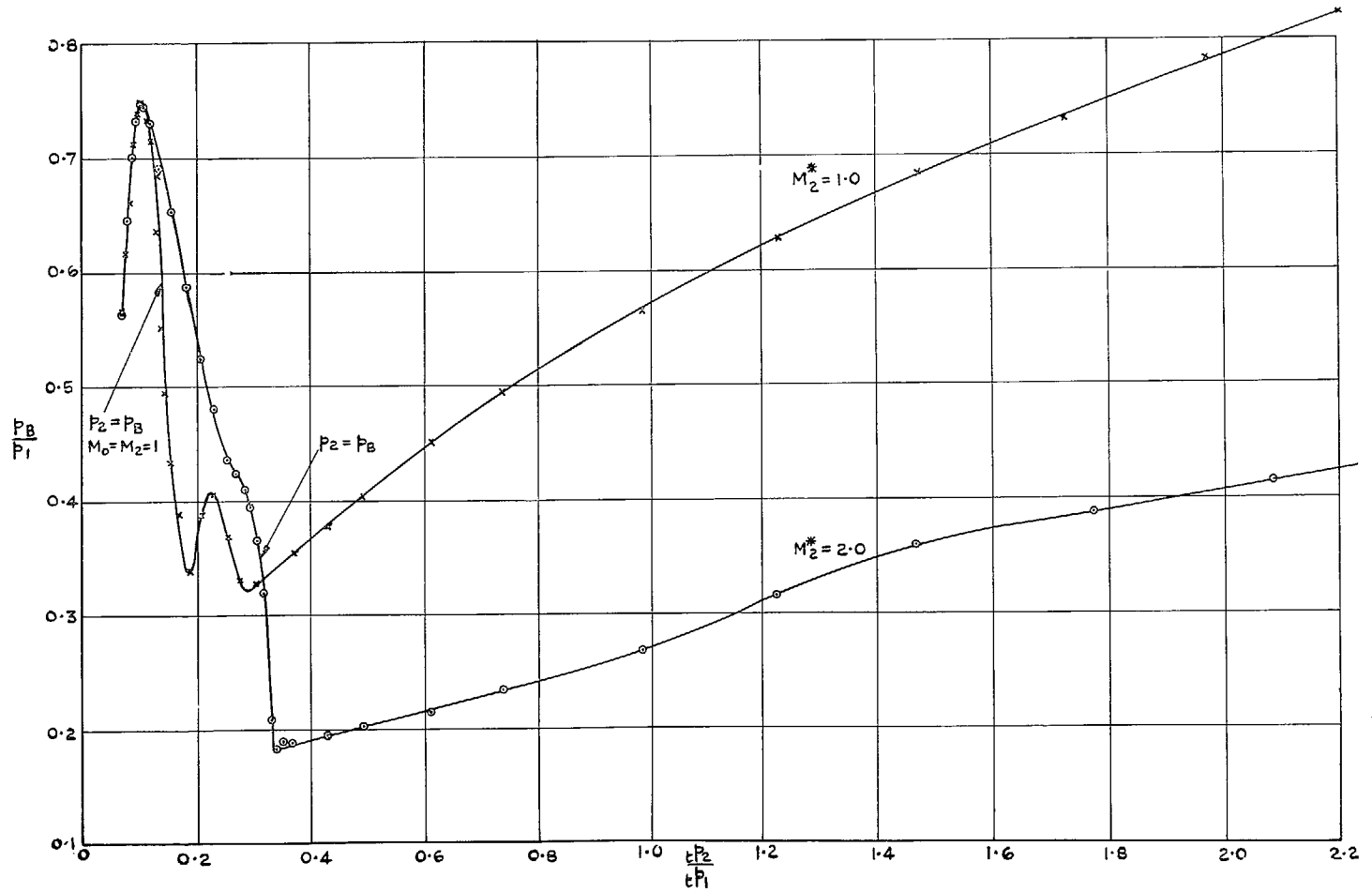


FIG. 11. The effect of nozzle design Mach number on base pressure.
 [$M_1 = 2.0$, $\beta_1 = 0$ deg, $\beta_2 = 0$ deg, $d_2/d_1 = 0.6$.]

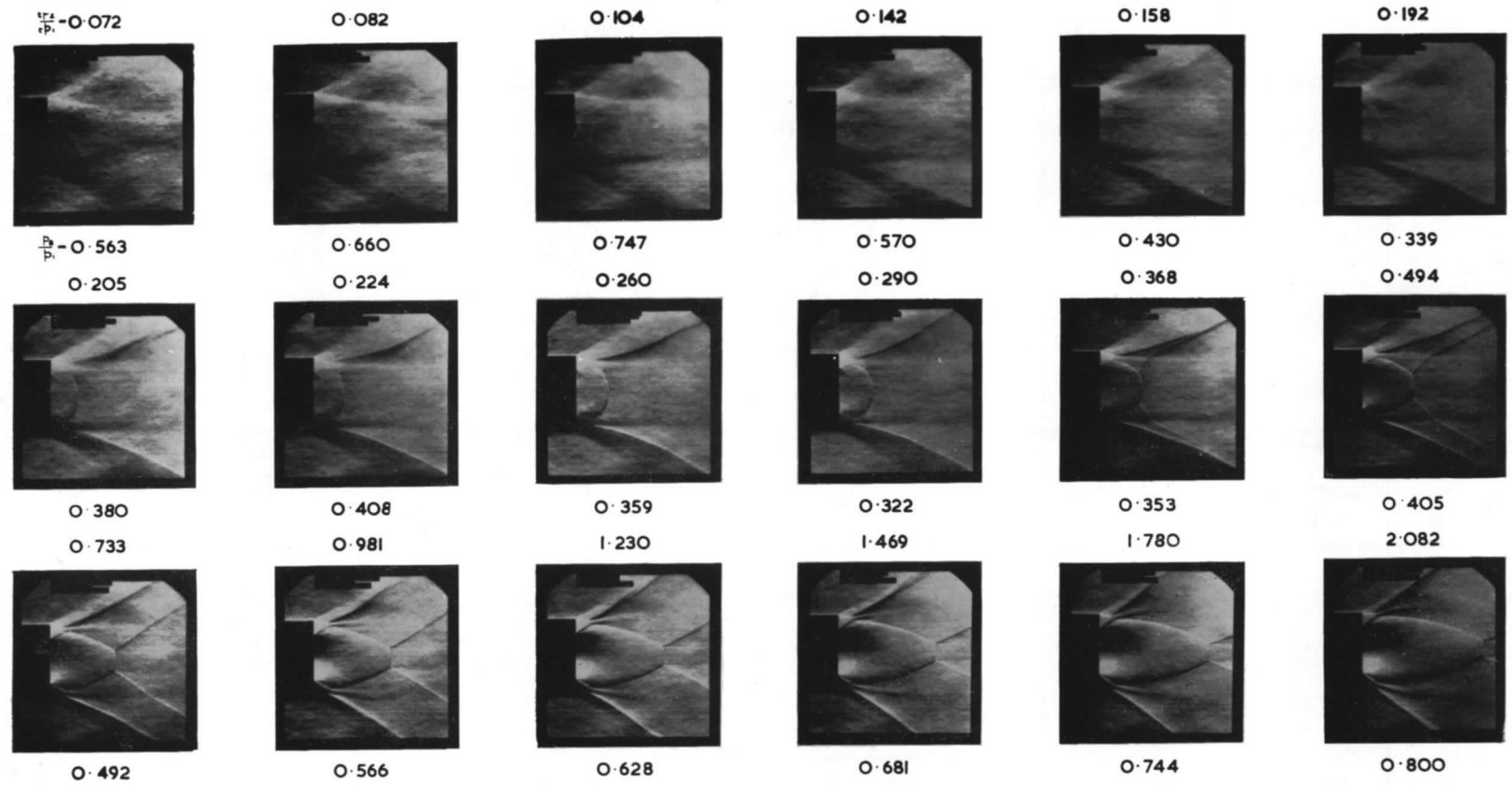


FIG. 12. Schlieren photographs showing the effect of jet pressure ratio on the base flow.
 Model No. 1-0-60. [$M_1 = 2.0$, $M_2^* = 1.0$, $\beta_1 = 0$ deg, $\beta_2 = 0$ deg, $d_2/d_1 = 0.6$.]

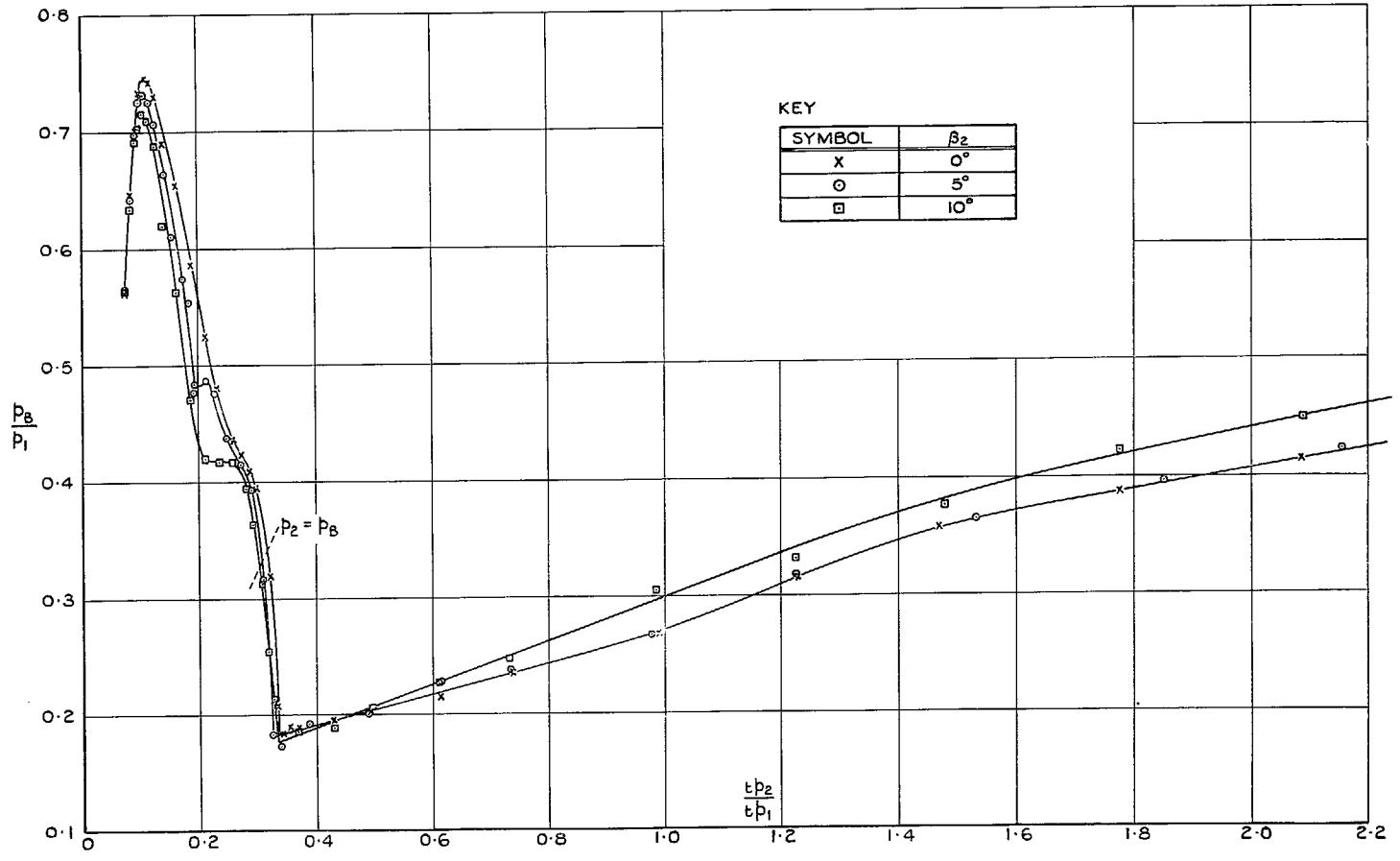


FIG. 13. The effect of nozzle divergence angle on base pressure.

[$M_1 = 2.0, M_2^* = 2.0, \beta_1 = 0 \text{ deg}, d_2/d_1 = 0.6.$]

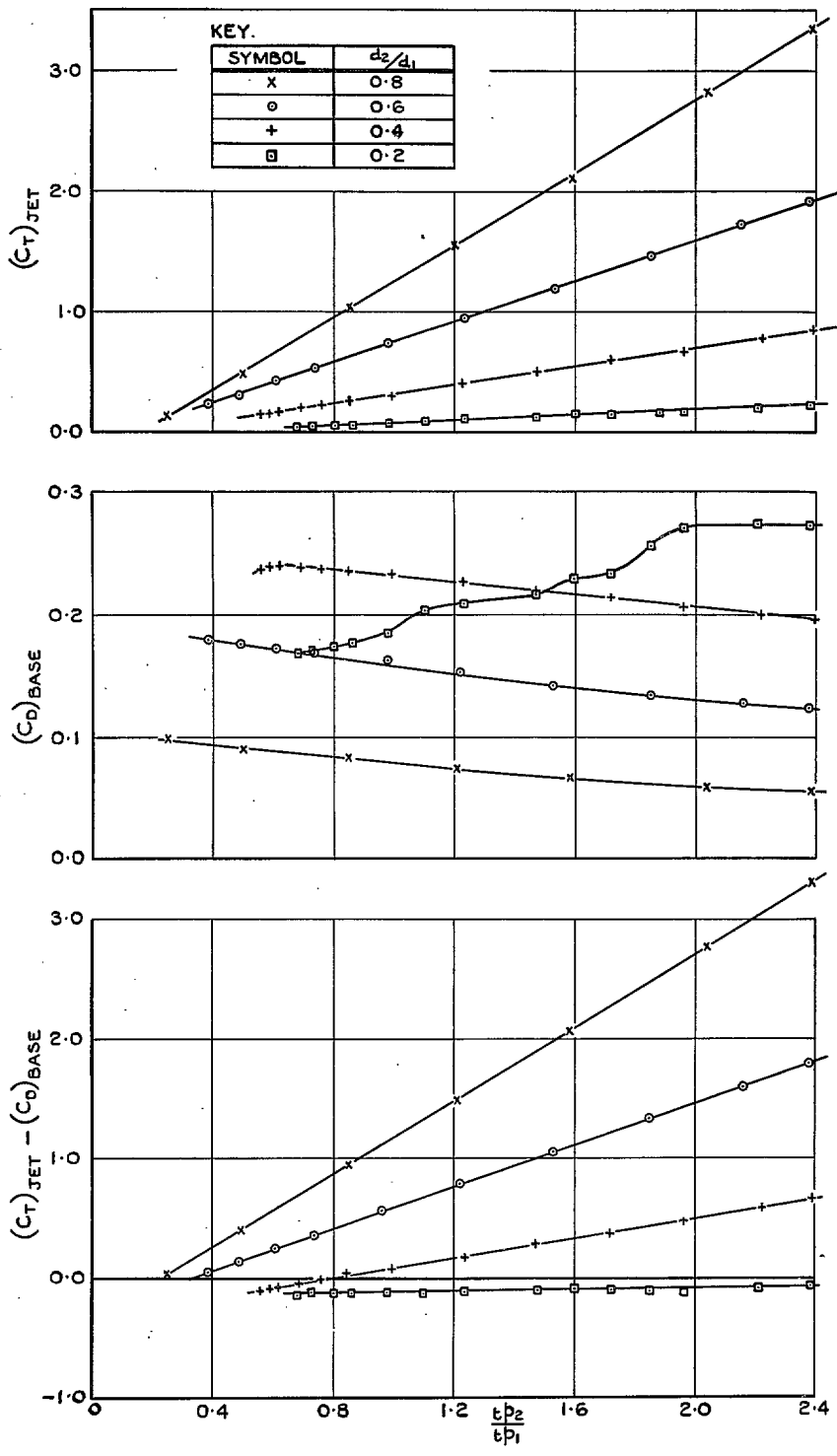


FIG. 14. The effect of jet/base diameter ratio on jet thrust and base drag.

[$M_1 = 2.0$, $M_2^* = 2.0$, $\beta_1 = 0$ deg, $\beta_2 = 5$ deg.]

NOTE :- THE CURVES \square ARE DERIVED FROM FIG.14 BY INTERPOLATION .

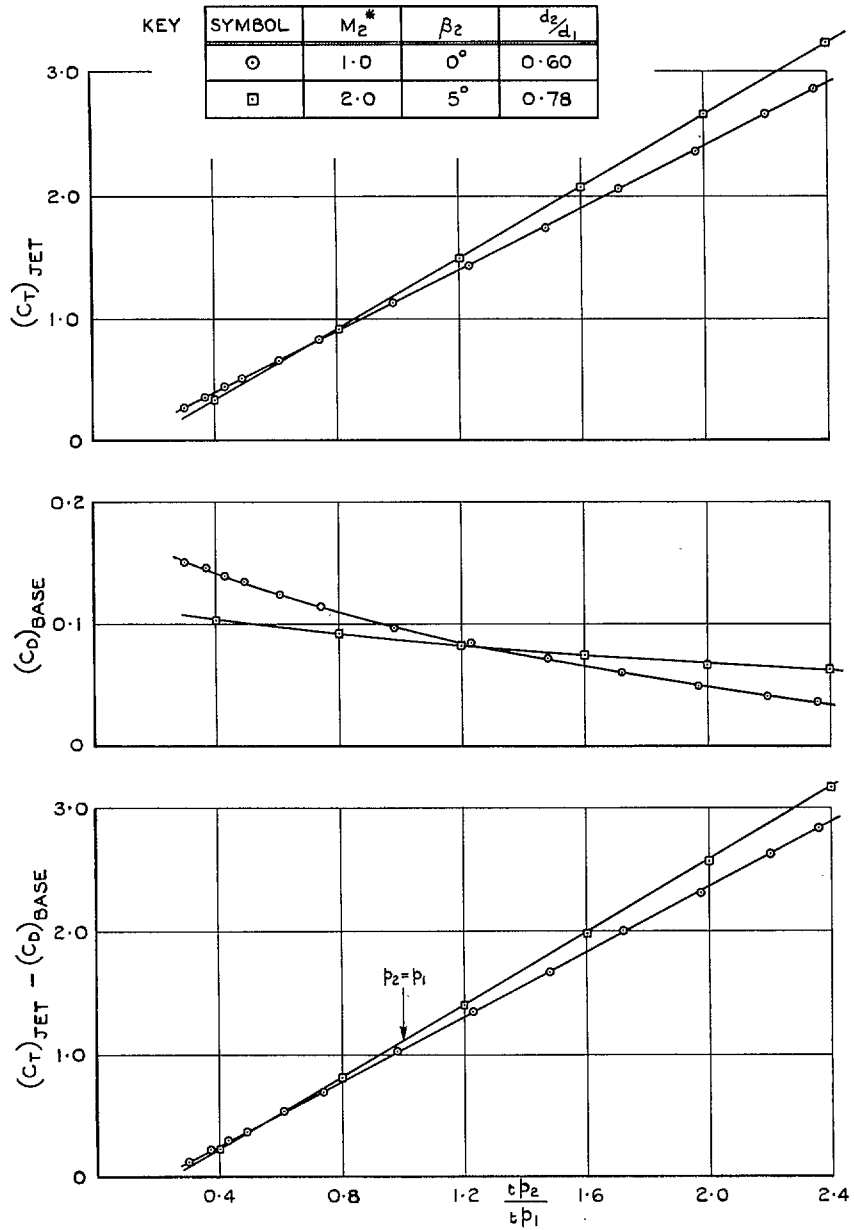


FIG. 15. The effect of nozzle design Mach number on jet thrust and base drag.

$[M_1 = 2.0, \beta_1 = 0 \text{ deg}, d_0/d_1 = 0.6.]$

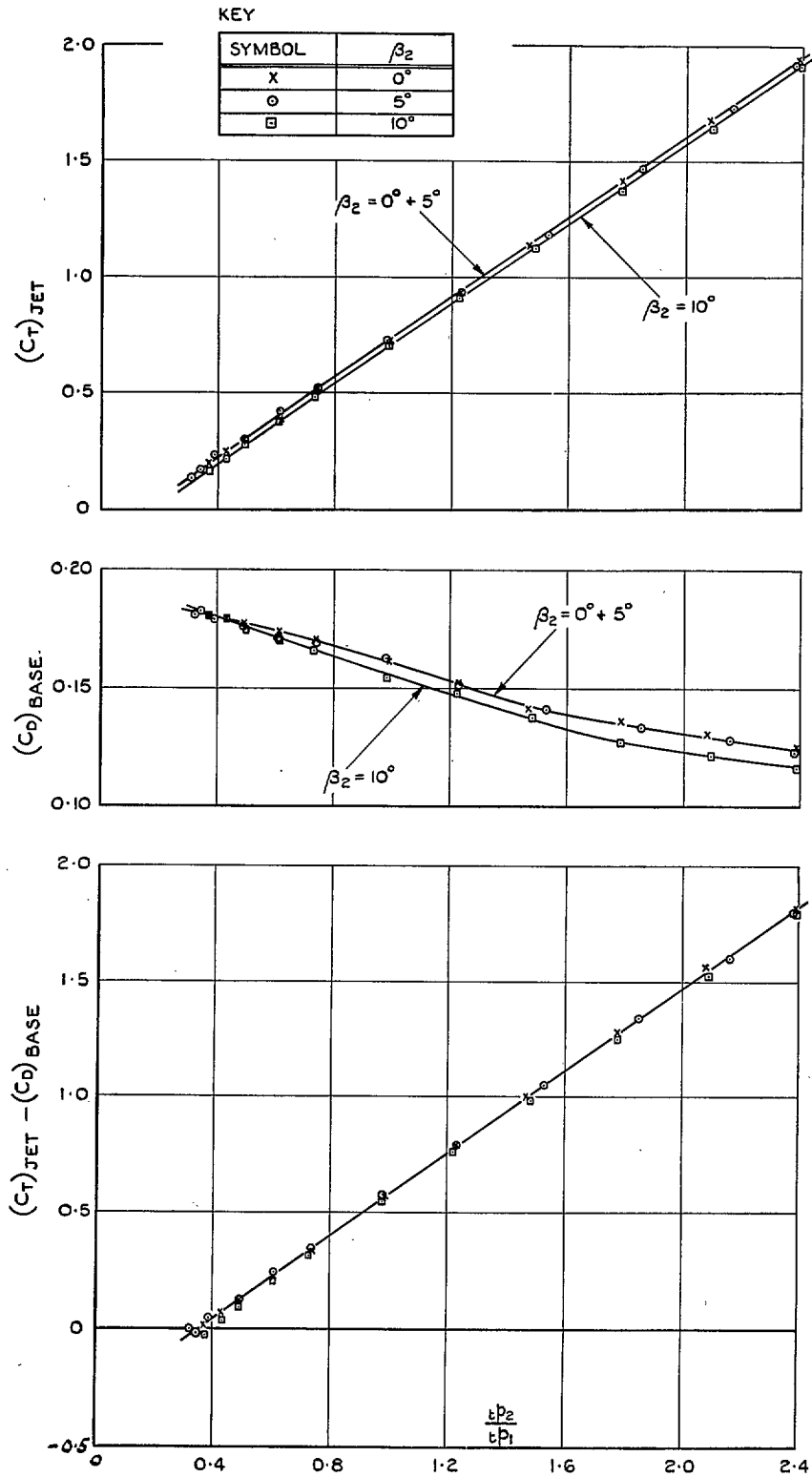
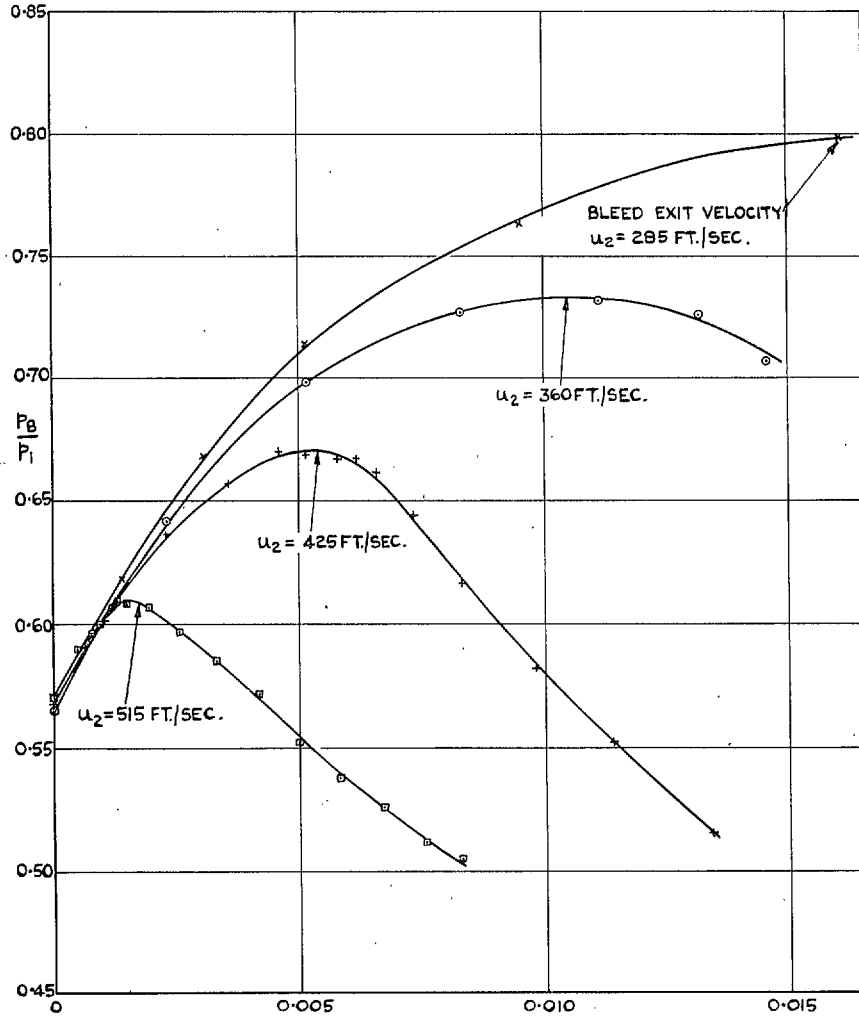


FIG. 16. The effect of nozzle divergence angle on jet thrust and base drag.

[$M_1 = 2.0$, $M_2^* = 2.0$, $\beta_1 = 0$ deg, $d_2/d_1 = 0.6$.]

KEY

SYMBOL	$\frac{d_2}{d_1}$
X	0.8
○	0.6
+	0.4
□	0.2



$$H = \sqrt{\frac{R}{\gamma}} \cdot \frac{q \sqrt{t_1}}{a_{1t} P_1}$$

FIG. 17. The effect of bleed mass flow and the ratio $\frac{\text{bleed exit dia.}}{\text{base dia.}} = \frac{d_2}{d_1}$ on the base pressure.

$[M_1 = 2.0, \beta_1 = 0 \text{ deg}, \beta_2 = 5 \text{ deg.}]$

NOTE:- (1) \odot DENOTES READING OF AMBIENT STATIC PRESSURE IN BASE.

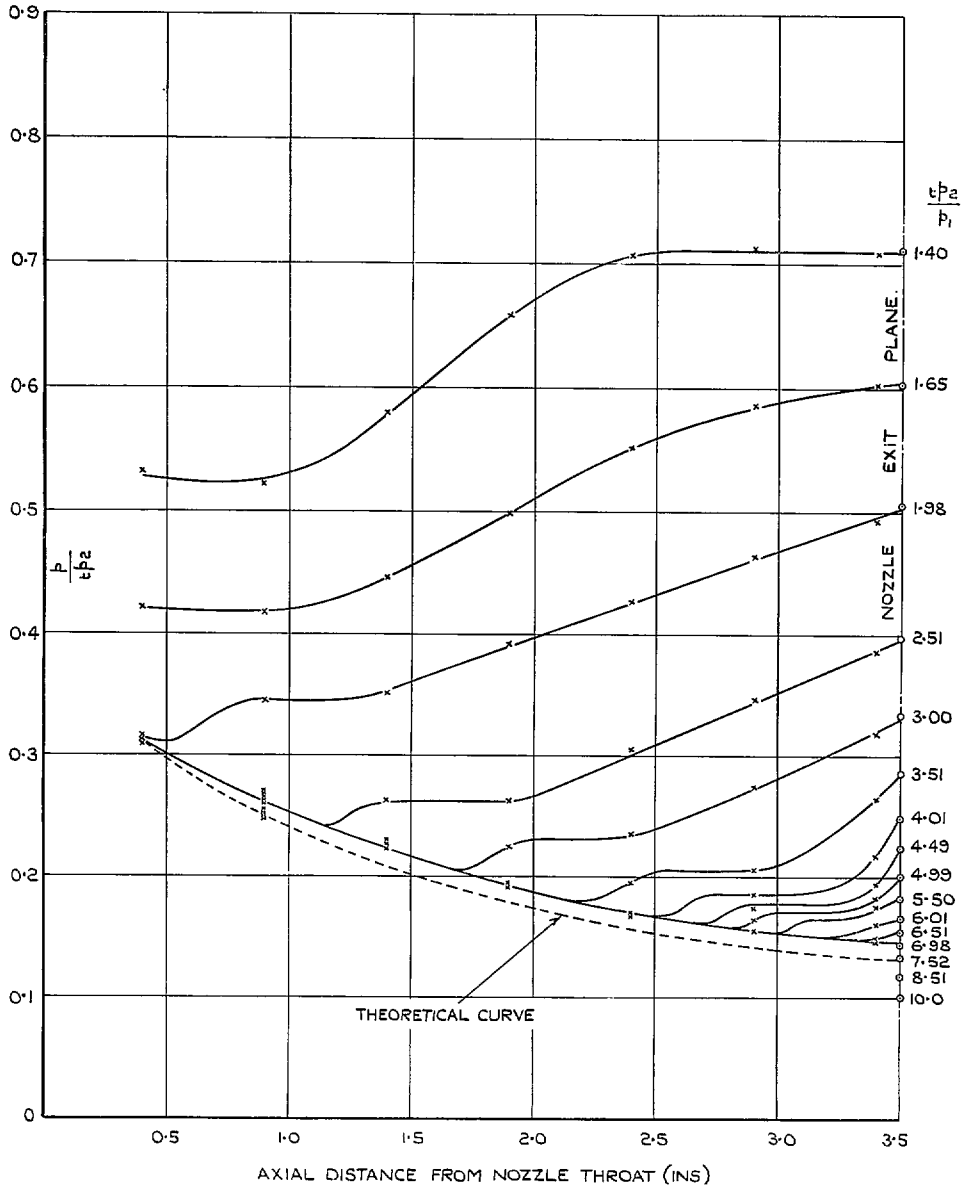


FIG. 18. The effect of jet pressure ratio on the pressure distribution inside the nozzle. Model No. 2-0-60. [$M_1 = 0$, $M_2^* = 2.0$, $\beta_2 = 0$ deg.]

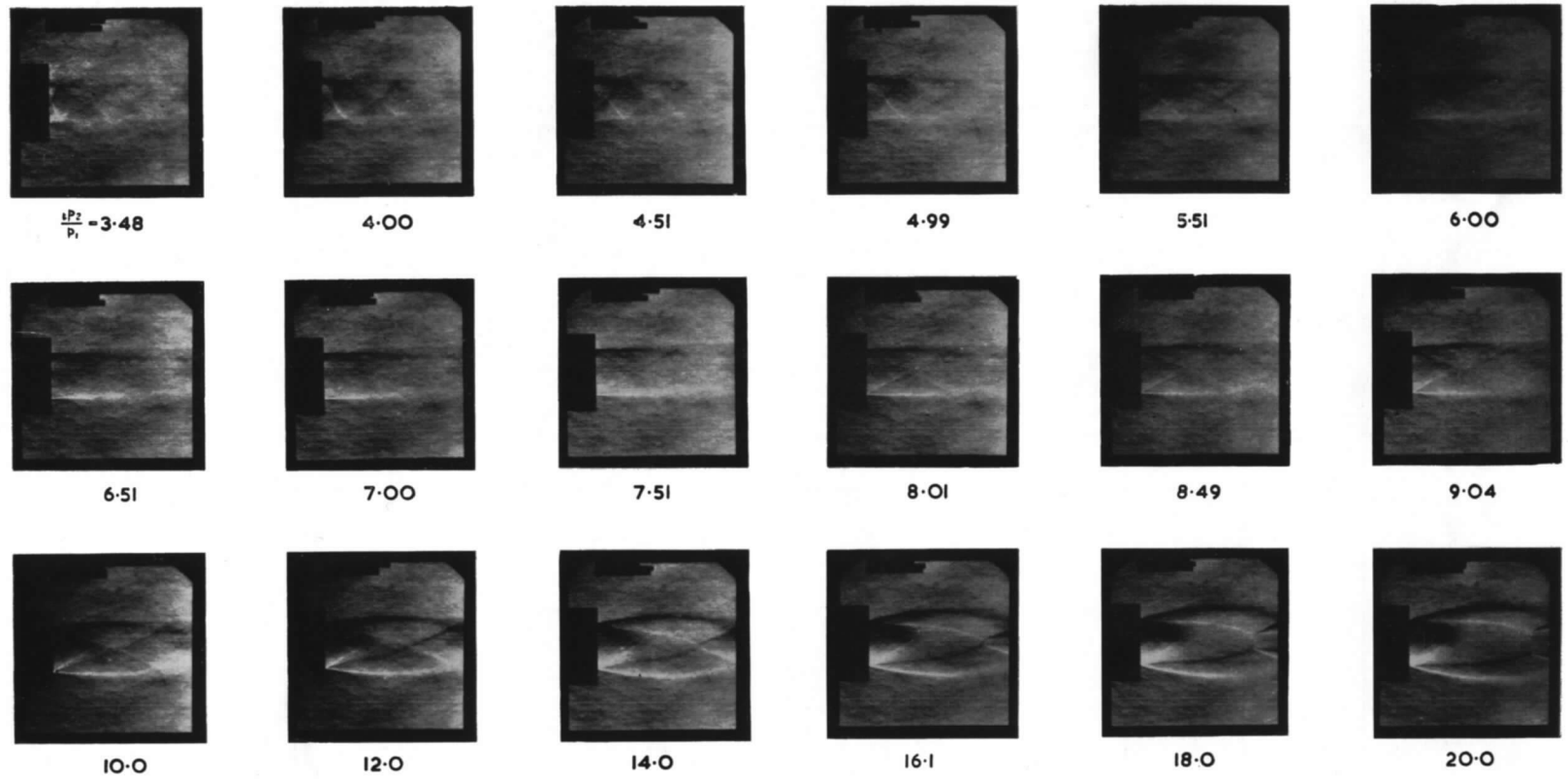


FIG. 19. Schlieren photographs showing the effect of jet pressure ratio on the jet structure.
 Model No. 2-0-60. [$M_1 = 0$, $M_2^* = 2.0$, $\beta_2 = 0$ deg.]

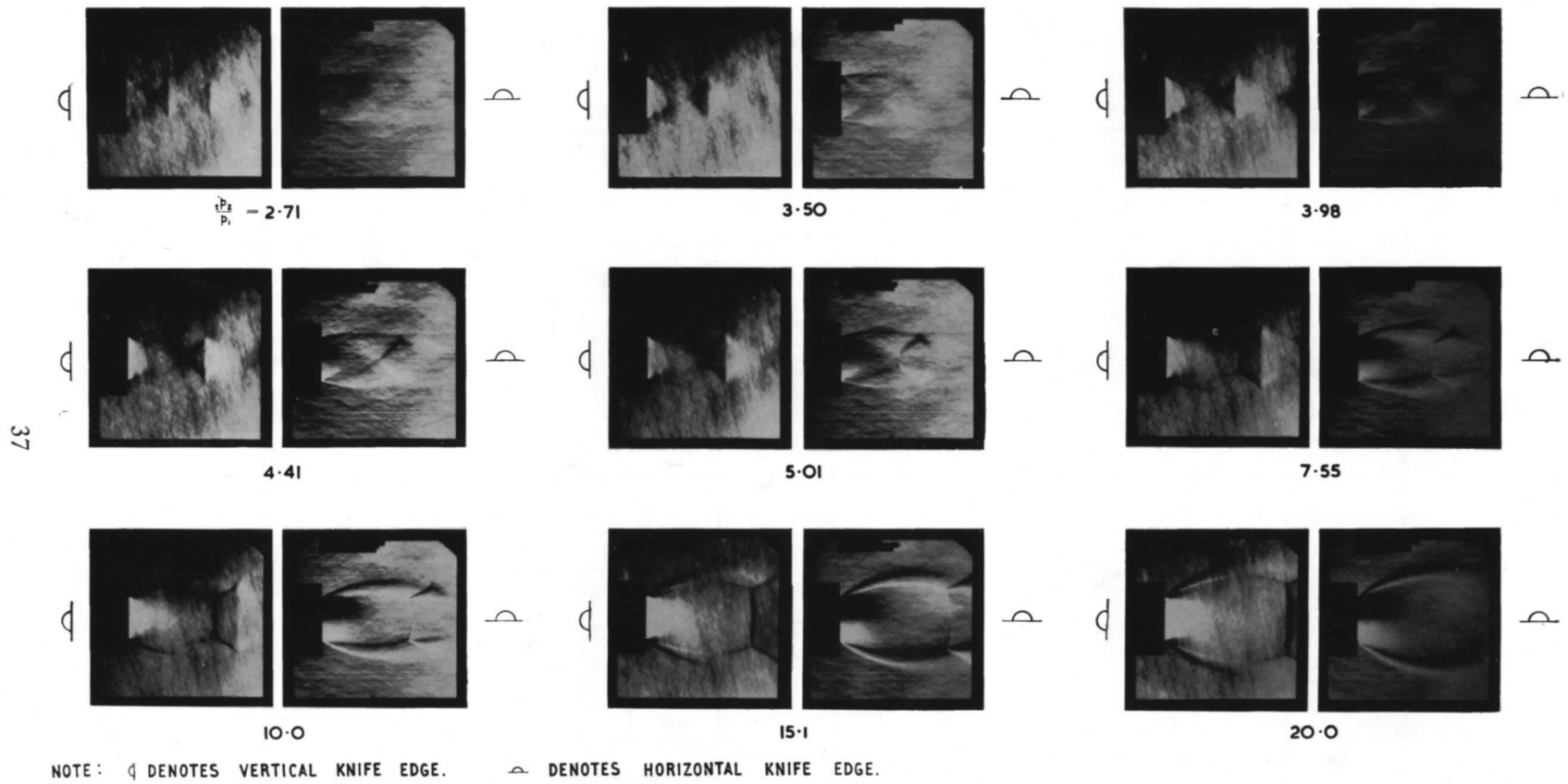


FIG. 20. Schlieren photographs showing the effect of jet pressure ratio on the jet structure.
 Model No. 1-0-60. [$M_1 = 0$, $M_2^* = 1.0$, $\beta_2 = 0$ deg.]

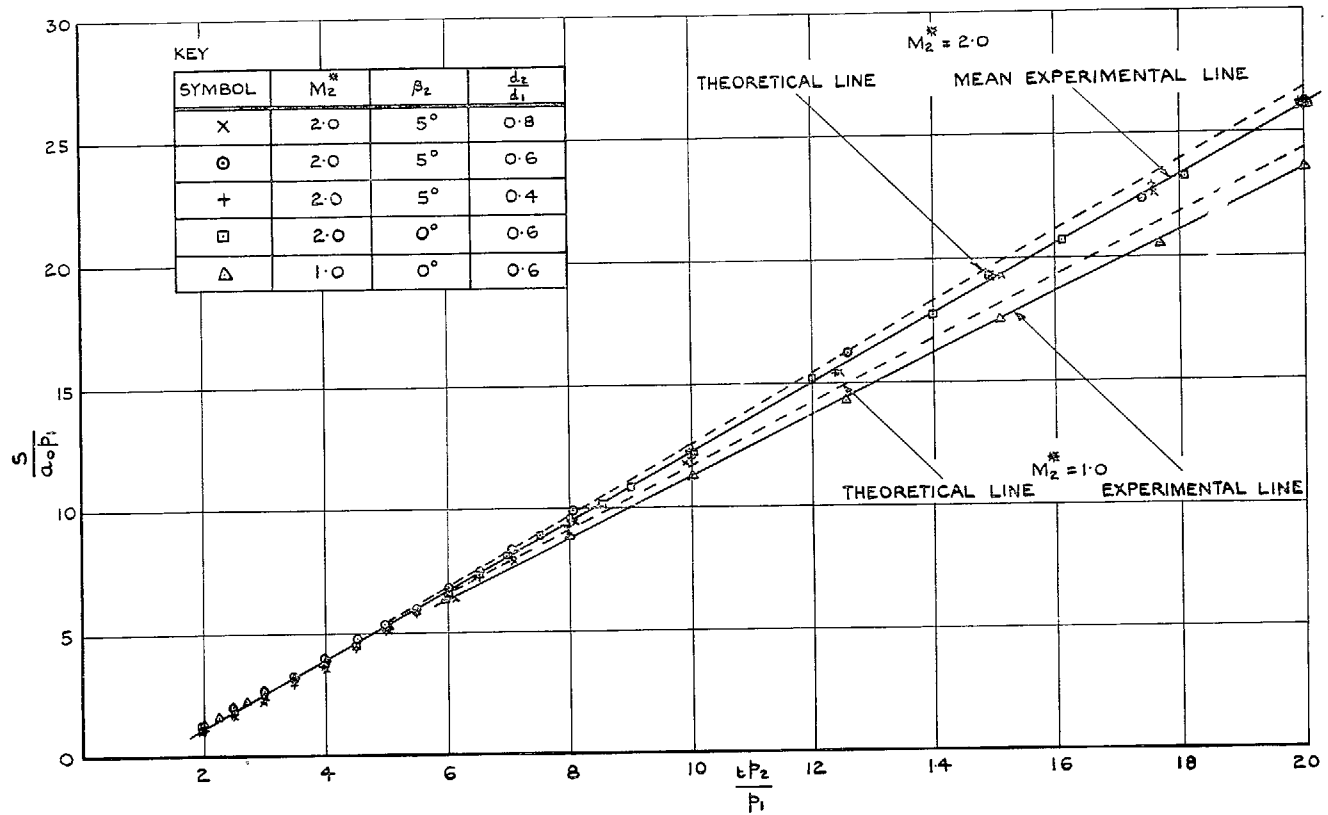


FIG. 21. The effect of jet pressure ratio on the thrust. ($M_1 = 0.$)

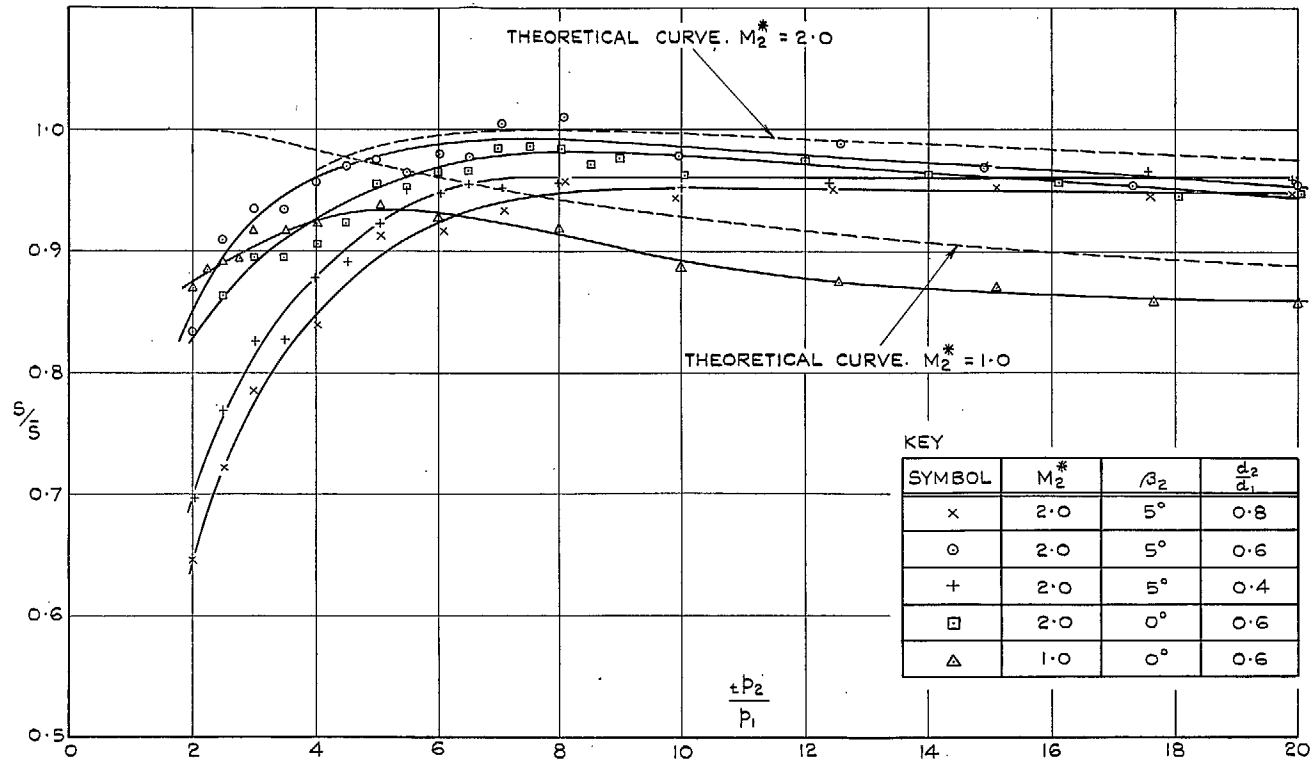


FIG. 22. The effect of jet pressure ratio on the thrust efficiency. ($M_1 = 0.$)

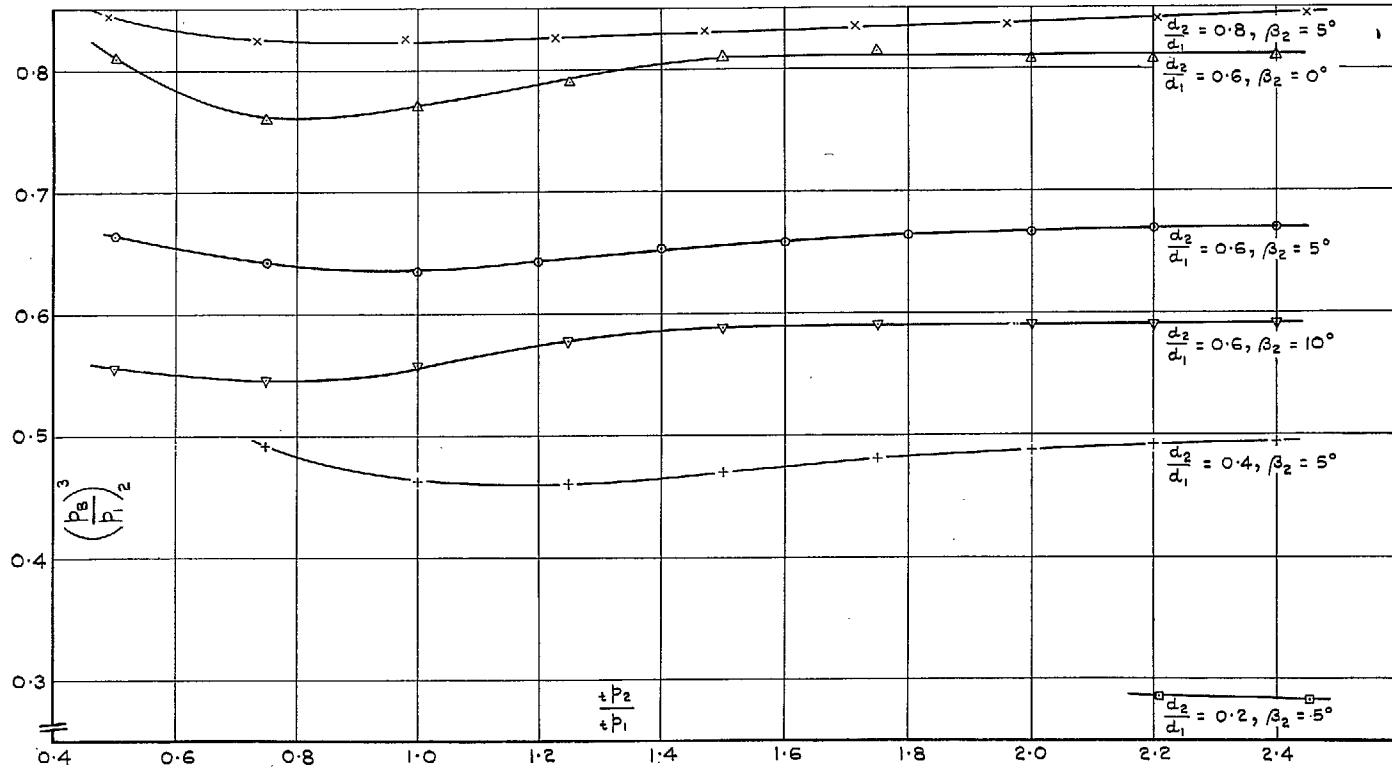


FIG. 23. Correlation of annular and two-dimensional base pressures. The effect of jet pressure ratio.

$[M_1 = 2.0, M_2 = 2.0, \beta_1 = 0 \text{ deg.}]$

NOTE:- THE SYMBOL \lceil DENOTES THE SPREAD IN $\left(\frac{p_2}{p_1}\right)^3$ OVER THE RANGE OF $\frac{t_{p_2}}{t_{p_1}}$ SHOWN IN FIG. 23.

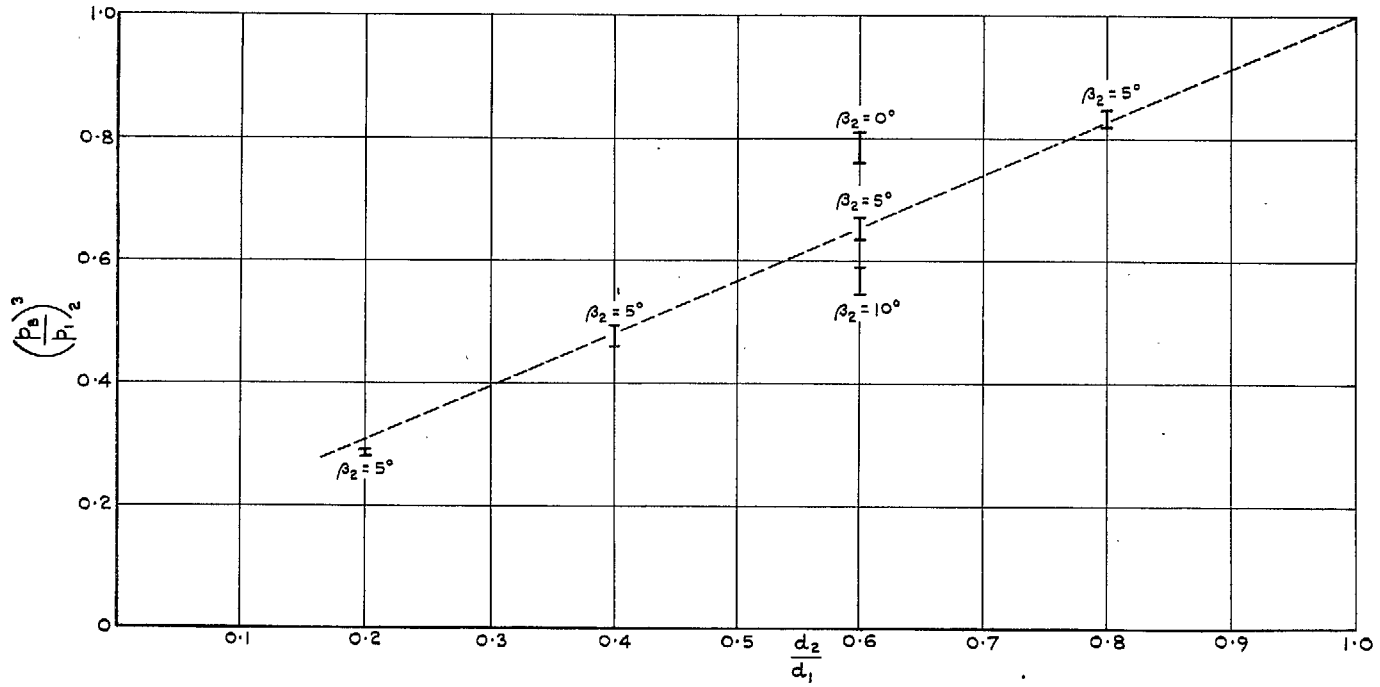


FIG. 24. Correlation of annular and two-dimensional base pressures. The effect of jet-base diameter ratio.
[$M_1 = 2.0$, $M_2 = 2.0$, $\beta_1 = 0$ deg.]

Publications of the Aeronautical Research Council

ANNUAL TECHNICAL REPORTS OF THE AERONAUTICAL RESEARCH COUNCIL (BOUND VOLUMES)

- 1941 Aero and Hydrodynamics, Aerofoils, Airscrews, Engines, Flutter, Stability and Control, Structures. 63s. (post 2s. 3d.)
- 1942 Vol. I. Aero and Hydrodynamics, Aerofoils, Airscrews, Engines. 75s. (post 2s. 3d.)
Vol. II. Noise, Parachutes, Stability and Control, Structures, Vibration, Wind Tunnels. 47s. 6d. (post 1s. 9d.)
- 1943 Vol. I. Aerodynamics, Aerofoils, Airscrews. 80s. (post 2s.)
Vol. II. Engines, Flutter, Materials, Parachutes, Performance, Stability and Control, Structures. 90s. (post 2s. 3d.)
- 1944 Vol. I. Aero and Hydrodynamics, Aerofoils, Aircraft, Airscrews, Controls. 84s. (post 2s. 6d.)
Vol. II. Flutter and Vibration, Materials, Miscellaneous, Navigation, Parachutes, Performance, Plates and Panels, Stability, Structures, Test Equipment, Wind Tunnels. 84s. (post 2s. 6d.)
- 1945 Vol. I. Aero and Hydrodynamics, Aerofoils. 130s. (post 3s.)
Vol. II. Aircraft, Airscrews, Controls. 130s. (post 3s.)
Vol. III. Flutter and Vibration, Instruments, Miscellaneous, Parachutes, Plates and Panels, Propulsion. 130s. (post 2s. 9d.)
Vol. IV. Stability, Structures, Wind Tunnels, Wind Tunnel Technique. 130s. (post 2s. 9d.)
- 1946 Vol. I. Accidents, Aerodynamics, Aerofoils and Hydrofoils. 168s. (post 3s. 3d.)
Vol. II. Airscrews, Cabin Cooling, Chemical Hazards, Controls, Flames, Flutter, Helicopters, Instruments and Instrumentation, Interference, Jets, Miscellaneous, Parachutes. 168s. (post 2s. 9d.)
Vol. III. Performance, Propulsion, Seaplanes, Stability, Structures, Wind Tunnels. 168s. (post 3s.)
- 1947 Vol. I. Aerodynamics, Aerofoils, Aircraft. 168s. (post 3s. 3d.)
Vol. II. Airscrews and Rotors, Controls, Flutter, Materials, Miscellaneous, Parachutes, Propulsion, Seaplanes, Stability, Structures, Take-off and Landing. 168s. (post 3s. 3d.)

Special Volumes

- Vol. I. Aero and Hydrodynamics, Aerofoils, Controls, Flutter, Kites, Parachutes, Performance, Propulsion, Stability. 126s. (post 2s. 6d.)
- Vol. II. Aero and Hydrodynamics, Aerofoils, Airscrews, Controls, Flutter, Materials, Miscellaneous, Parachutes, Propulsion, Stability, Structures. 147s. (post 2s. 6d.)
- Vol. III. Aero and Hydrodynamics, Aerofoils, Airscrews, Controls, Flutter, Kites, Miscellaneous, Parachutes, Propulsion, Seaplanes, Stability, Structures, Test Equipment. 189s. (post 3s. 3d.)

Reviews of the Aeronautical Research Council

1939-48 3s. (post 5d.) 1949-54 5s. (post 5d.)

Index to all Reports and Memoranda published in the Annual Technical Reports

1909-1947 R. & M. 2600 6s. (post 2d.)

Indexes to the Reports and Memoranda of the Aeronautical Research Council

Between Nos. 2351-2449	R. & M. No. 2450 2s. (post 2d.)
Between Nos. 2451-2549	R. & M. No. 2550 2s. 6d. (post 2d.)
Between Nos. 2551-2649	R. & M. No. 2650 2s. 6d. (post 2d.)
Between Nos. 2651-2749	R. & M. No. 2750 2s. 6d. (post 2d.)
Between Nos. 2751-2849	R. & M. No. 2850 2s. 6d. (post 2d.)
Between Nos. 2851-2949	R. & M. No. 2950 3s. (post 2d.)
Between Nos. 2951-3049	R. & M. No. 3050 3s. 6d. (post 2d.)

HER MAJESTY'S STATIONERY OFFICE

from the addresses overleaf

© *Crown copyright* 1961

Printed and published by
HER MAJESTY'S STATIONERY OFFICE

To be purchased from
York House, Kingsway, London W.C.2
423 Oxford Street, London W.1
13A Castle Street, Edinburgh 2
109 St. Mary Street, Cardiff
39 King Street, Manchester 2
50 Fairfax Street, Bristol 1
2 Edmund Street, Birmingham 3
80 Chichester Street, Belfast 1
or through any bookseller

Printed in England